

LOW COST DEFORMATION ANALYSIS OF OPEN PIT MINE BY USING
UNMANNED AERIAL VEHICLE (UAV) TECHNOLOGY

A THESIS SUBMITTED TO
THE GRADUATE SCHOOL OF NATURAL AND APPLIED SCIENCES
OF
MIDDLE EAST TECHNICAL UNIVERSITY

BY

GÖKTUĞ SÖĞÜTCÜ

IN PARTIAL FULFILLMENT OF THE REQUIREMENTS
FOR
THE DEGREE OF MASTER OF SCIENCE
IN
GEOLOGICAL ENGINEERING

JANUARY 2024

Approval of the thesis:

**LOW-COST DEFORMATION ANALYSIS OF OPEN PIT MINE BY USING
UNMANNED AERIAL VEHICLES (UAV) TECHNOLOGY**

submitted by **GÖKTUĞ SÖĞÜTCÜ** in partial fulfillment of the requirements for
the degree of **Master of Science in Geological Engineering, Middle East
Technical University** by,

Prof. Dr. Halil Kalıpçılar
Dean, Graduate School of **Natural and Applied Sciences**

Prof. Dr. Erdin Bozkurt
Head of the Department, **Geological Engineering**

Prof. Dr. Mehmet Lütfi Süzen
Supervisor, **Geological Engineering, METU**

Prof. Dr. Tolga Görüm
Co-Supervisor, **Eurasia Institute of Earth Sciences, ITU**

Examining Committee Members:

Prof. Dr. Aykut Akgün
Geological Eng., KTU

Prof. Dr. M. Lütfi Süzen
Geological Eng., METU

Prof. Dr. Tolga Görüm
Eurasia Institute of Earth Sciences, ITU

Prof. Dr. Ali Özgün Ok
Geomatics Eng., Hacettepe Uni.

Assoc. Prof. Dr. Koray K. Yılmaz
Geological Eng., METU

Date: 26.01.2024

I hereby declare that all information in this document has been obtained and presented in accordance with academic rules and ethical conduct. I also declare that, as required by these rules and conduct, I have fully cited and referenced all material and results that are not original to this work.

Name Last name : Gökтуğ Söğütçü

Signature :

ABSTRACT

LOW-COST DEFORMATION ANALYSIS OF OPEN PIT MINE BY USING UNMANNED AERIAL VEHICLE (UAV) TECHNOLOGY

Söğütçü, Gökтуğ
Master of Science, Geological Engineering
Supervisor: Prof. Dr. Mehmet Lütfi Süzen
Co-Supervisor: Prof. Dr. Tolga Görüm

January 2024, 57 pages

Geotechnical engineers are authorized people to assess the stability of any structure in mining projects as in the other engineering projects such as tunnel, motorway or dam construction, etc. In those projects, deformation analysis is critical for geotechnical works because any failure, or major landslides that may occur in the projects can cause pecuniary or non-pecuniary damages. Therefore, geotechnical engineers have been using many monitoring tools like Slope Stability RADAR, Robotic Total Station, InSAR, extensometer and inclinometers. However, those instruments require high initial investment and require stable environments to establish a baseline in the beginning period of a lot of mining projects, where this situation directs companies and engineers to find alternative solutions for monitoring. Unmanned Aerial Vehicles (UAV) are one of those alternatives to perform slope stability assessment in a cheap and reliable way. Thus, the usage of those are increasing in mining operations and other engineering fields progressively.

In this thesis, the UAV's are used to make a 3D change detection analysis and instability assessment map of an open pit by using free open-source softwares. As a result of these analyses, it is clearly presented that the instabilities are small-scale,

and the maximum displacement is -2.41m in the studied area. An instability assessment map is created to specify the susceptible zones by using some significant criteria that may affect the stability in the pit. This thesis aims to present how geotechnical engineers can detect deformation regions in an open pit by using UAVs.

Keywords: Unmanned Aerial Vehicle (UAV), Monitoring, Change Detection, Slope Instability

ÖZ

AÇIK OCAK MADENİNİN İNSANSIZ HAVA ARACI (İHA) TEKNOLOJİSİYLE DÜŞÜK MALİYETLİ DEFORMASYON ANALİZİ

Söğütçü, Göktuğ
Yüksek Lisans, Jeoloji Mühendisliği
Tez Yöneticisi: Prof. Dr. Mehmet Lütfi Süzen
Ortak Tez Yöneticisi: Prof. Dr. Tolga Görüm

Ocak 2024, 57 sayfa

Jeoteknik mühendisleri tünel inşaatı, otoyol inşaatı, baraj inşaatı vb. mühendislik projelerinde olduğu gibi madencilik projelerinde de herhangi bir yapının duraylılığını kontrol etmeye yetkili kişilerdir. Bu projelerde, herhangi bir yenilme veya büyük heyelan nedeniyle deformasyon analizi jeoteknik çalışmalar için kritik öneme sahiptir. Projelerde meydana gelebilecek olaylar maddi veya manevi zararlara yol açabilmektedir. Bu nedenle jeoteknik mühendisleri Şev Stabilite RADAR'ı, Robotic Total Station, InSAR, ekstensometre ve eğimölçerler gibi birçok izleme aracını kullanmaktadır. Ancak bu araçlar için yüksek başlangıç yatırımı ve duraylı sahalar, birçok madencilik projesinin başlangıç döneminde bir temel oluşturmak için gereklidir. Bu durum, şirketleri ve mühendisleri izleme için alternatif çözümler bulmaya yönlendirmektedir. İnsansız Hava Araçları (İHA), şev duraylılığı değerlendirmesini ucuz ve güvenilir bir şekilde gerçekleştirmenin alternatiflerinden biridir. Bu nedenle madencilik faaliyetlerinde ve diğer mühendislik alanlarında bunların kullanımını giderek artmaktadır.

Bu tezde İHA'lar, ücretsiz açık kaynaklı yazılımlar kullanılarak bir açık ocağın 3 boyutlu değişim tespit analizi ve duraysızlık değerlendirme haritasının yapılması için

kullanılmıştır. Bu analizler sonucunda duraysızlıkların küçük ölçekli olduđu ve çalışılan alanda maksimum yer deđiřtirmenin -2.41m olduđu açıkça ortaya konmuřtur. Ocaktaki duraylılıđı etkileyebilecek bazı önemli kriterler kullanılarak hassas bölgelerin belirlenmesi amacıyla bir duraysızlık deđerlendirme haritası oluşturulmuřtur. Bu tez, jeoteknik mühendislerinin açık ocaktaki deformasyon bölgelerini İHA kullanarak nasıl tespit edebileceklerini sunmayı amaçlamaktadır.

Anahtar Kelimeler: İnsansız Hava Aracı (İHA), İzleme, Deđerşim Tespiti, Şev Duraysızlıđı

To my parents and my friends who never leave me alone...

ACKNOWLEDGMENTS

I would like to express my sincere gratitude to my supervisor Prof. Dr. Mehmet Lütfi Süzen and co-supervisor Prof. Dr. Tolga Görüm for their guidance, advice, criticism, encouragement, and insight throughout the research.

I would also like to thank my dear brother Mustafa Yurtsever for introducing me to drone technology and the photogrammetry process for the first time. Thanks to his help, I had a chance to improve myself and complete my thesis study.

My most appreciation goes to my mother Gülten Söğütçü and all my friends who always supported me and believed in me.

TABLE OF CONTENTS

ABSTRACT.....	v
ÖZ.....	vii
ACKNOWLEDGMENTS	x
TABLE OF CONTENTS.....	xi
LIST OF TABLES	xiii
LIST OF FIGURES	xiv
LIST OF ABBREVIATIONS	xvii
CHAPTERS	
1 INTRODUCTION	1
1.1 Purpose and Scope of the Study.....	2
1.2 Study Area	2
1.3 Geological Background	3
2 LITERATURE REVIEW	5
2.1 Multitemporal analyses with UAVs for change detection	5
2.2 Multicriteria Analysis in GIS Environment	8
3 METHODOLOGY	11
3.1 Preparation of Flight Path	11
3.2 Selection of Ground Control Points (GCPs).....	12
3.3 Photogrammetric Processes	13
3.4 Data Analyses	16
3.4.1 3D Change Detection Analysis with the Point Cloud Sets	17
3.4.2 The Comparison between Photogrammetric Data and SSR Data	23

3.4.3	Failure Frequency in the Alteration Zones	32
3.4.4	Volume Calculation for Deposited Material on the Benches	35
3.4.5	Tension Crack Mapping.....	36
3.4.6	Creation of Slope Map	37
4	INSTABILITY ASSESSMENT MAPPING.....	39
4.1	Criteria.....	39
4.2	Creation of Instability Assessment Map in QGIS	45
4.3	Accuracy Assessment of Instability Assessment Map	47
5	RESULTS AND DISCUSSION.....	49
5.1	Change Detection Analyses.....	49
5.2	The Volume Calculation for Accumulated Material	49
5.3	Types of Alteration.....	49
5.4	Performance of Low-Cost UAV to monitor Mining Sites	50
5.5	Stability Status on Different Types of Alteration.....	51
5.6	Negative Effects of Tension Cracks on Slope Stability	51
5.7	The Volume Accumulation on the Benches	51
6	CONCLUSION	53
	REFERENCES	55

LIST OF TABLES

TABLES

Table 3.1 Summary information of each survey data	16
Table 4.1 Summary of the classification and reclassification details of the criteria	45
Table 4.2 Pairwise Comparison Matrix for the datasets and criteria weight results	46
Table 4.3 Descriptions and their class intervals for Instability Assessment Map...	46

LIST OF FIGURES

FIGURES

Figure 1.1. Location of study area in the open pit (Kayseri city, Türkiye)	3
Figure 3.1. The methodology of the study.	11
Figure 3.2. Flight path for the target zone in “DJI Terra” software.	12
Figure 3.3. Ground Control Points in the study area.	13
Figure 3.4. The parameters that represent the processes of the generation of point cloud, DEM and orthomosaic in the Agisoft Metashape interface.	14
Figure 3.5. a) The dense point cloud, b) Digital Elevation Model, c) Orthomosaic generated in Agisoft Metashape Professional software.....	15
Figure 3.6. The phases of the data analyses	17
Figure 3.7. a) Colored-point dense cloud for 19.12.2022 (red dash lines represent the displacement caused by operational process). b) 3D change detection with M3C2 method in the dates between 08.09.2022-19.12.2022	19
Figure 3.8. a) Colored-point dense cloud for 24.01.2023. (red dash lines represent the displacement caused by operational process). b) 3D change detection with M3C2 method in the dates between 08.09.2022-24.01.2023	20
Figure 3.9. a) Colored-point dense cloud for 07.03.2023 (red dash lines represent the displacement caused by operational process). b) 3D change detection with M3C2 method in the dates between 08.09.2022-07.03.2023	21
Figure 3.10. a) Colored-point dense cloud for 26.06.2023 (red dash lines represent the displacement caused by operational process). b) 3D change detection with M3C2 method in the dates between 08.09.2022-26.06.2023	22
Figure 3.11. a) Point cloud data of M3C2 distance method in between 08/09/2022 and 26/06/2023. b) Point cloud data (relative range) of SSR in between 08/09/2022 and 26/06/2023. c) The image draped point cloud data in 26/06/2023 and red dash lines represent the regions where small-scale failures occurred.....	24

Figure 3.12. a) The relative range data of SSR and the transformation of point cloud data to raster data by using TIN interpolation. b) M3C2 distance data and the transformation of point cloud data to raster data by using TIN interpolation.....	25
Figure 3.13. a) The line of profile A-B on the map. b) The profile A-B.	26
Figure 3.14. The longitudinal profile lines on the map.....	27
Figure 3.15. (a) Displacement graph of profile 1, (b) profile 2.	28
Figure 3.16. (a) Displacement graph of profile 3, (b) profile 4.	29
Figure 3.17. Histograms of SSR and photogrammetric data based on the percentage of point cloud data which represents the failure points in the argillic alteration zone.	30
Figure 3.18. a) The location of the profile line used in the swath profile on the map, b) the swath profile of SSR based data (08/09/2022-26/06/2023), c) the swath profile of Drone based data (08/09/2022-26/06/2023).	31
Figure 3.19. Failure polygons acquired from height differences using DEM data between a) 08/09/2022-19/12/2022, b) 08/09/2022-24/01/2023, c) 08/09/2022-07/03/2023, d) 08/09/2022-26/06/2023.	33
Figure 3.20. Centroid points of failure polygons in the time interval between a) 08/09/2022 – 19/12/2022, b) 08/09/2022 – 24/01/2023, c) 08/09/2022 – 07/03/2023, d) 08/09/2022 – 26/06/2023.....	33
Figure 3.21. Alteration map of the study area.....	34
Figure 3.22. Number of centroid points of each failure polygons in each time interval.	34
Figure 3.23. The centroid points of failure polygons which belong to last epoch in argillic alteration - type 1 with tension cracks.	35
Figure 3.24. Volume calculation of deposited material on the benches.	36
Figure 3.25. a) The distribution of tension cracks around region 1. b) Bench-scale failure caused by the tension crack in region 1. c) The distribution of tension cracks in region 2. d) The overall view of region 1 and region 2.	37
Figure 3.26. a) Slope map generated from DEM of last epoch. b) Revised slope map.....	38

Figure 4.1. a) Alteration type of the study area. b) Reclassified map of Alteration Type.	40
Figure 4.2. a) Raster data of the slope angle. b) Reclassified map of Slope Angle.	41
Figure 4.3. a) Kernel density estimation of tension crack. b) Reclassified map of tension crack.	42
Figure 4.4. a) Vector data of the volume of accumulated material. b) Reclassified map of the volume of accumulated material.	43
Figure 4.5. a) Raster data of failure concentration. b) Reclassified map of failure concentration.	44
Figure 4.6. Instability Assessment Map.	47
Figure 4.7. Accuracy Assessment of Instability Assessment Map.	48

LIST OF ABBREVIATIONS

ABBREVIATIONS

UAV : Unmanned Aerial Vehicle

AHP : Analytical Hierarchy Process

M3C2 : Multiscale Model-to-Model Cloud Comparison

MCDA: Multi Criteria Decision Analysis

DEM : Digital Elevation Model

SSR : Slope Stability RADAR

SfM : Structure from Motion

GIS : Geographic Information System

CHAPTER 1

INTRODUCTION

Slope instability issues and ground subsidence which cause the surface deformations are very common events in the mining areas (Younger, 2007). The operations in open pit mine can trigger surface instabilities or various failures, and this can result in some risks to personnel and equipment affecting mine scheduling with rising production cost (Paradella et al., 2015). Therefore, the regular slope monitoring is necessary to provide safety of operations in open pit mine.

There are many techniques for slope monitoring like total station from subsurface techniques and subsurface techniques like inclinometers, extensometers, etc. (Vaziri et al., 2010). Besides this, remote monitoring technologies like Time Domain Reflectometry (TDR), scanners and RADAR (Osasan & Afeni, 2010). In addition, the use of UAV increases in mining sites day by day. UAV provides rich and reliable data in a highly precise and time efficient way in mining sites (Ren et al., 2019).

In mining operations, although there are many monitoring tools such as RADAR, total station for prism measurements, inclinometers etc, some technical problems that may occur on these devices can cause the loss of data, and prevent the geotechnical engineers to obtain information about stability in overall side of the pit. In addition, weather and seasonal conditions can also affect the data access negatively or these tools stop working for any technical issues. Therefore, alternative monitoring techniques should be developed to operate promptly in available meteorological windows which would increase the measurement periods and ease unmonitored period, and continue to monitoring without time and data loss.

1.1 Purpose and Scope of the Study

Unmanned Aerial Vehicle (UAV) systems are very helpful tools for the engineering field to monitor the open pit in a fast and practical way, and its implementation in the mining operations increases each passing day. In this study, an open pit with small-scale instability issues is targeted to evaluate the capabilities of low-cost drone technology in a mining site. Therefore, change detection analyses are firstly performed with point cloud sets derived from UAV in Cloud Compare software to monitor the open pit and then, an instability assessment map is created to observe critical areas in a single map by using free and open source geographic information system software (QGIS).

This thesis aims to create and test cost-effective deformation analysis in an open pit by acquiring data sets of change detection between point clouds created in different time intervals and determining the capabilities of low-cost drone technology by comparing with a slope stability RADAR (SSR). In addition, an instability assessment map is created to assess the eastern pit slopes with the data produced from UAV measurements.

This study might serve as an example to monitor open pits, concerning time and cost-effectiveness for the geotechnical engineers in the absence of other monitoring tools or in the breakdown of those expensive devices.

1.2 Study Area

The study area is conducted in an open pit. It is located in Central Anatolia, 50 km far from Kayseri province and 10 km from Develi town. The closest villages to the area are Öksüt, Epçe and Zile respectively. The east part of the pit is targeted to detect the existing slope failures and to make a deformation analysis in the zone (Figure 1.1).

The continental climate is seen in Develi town which means that the summers are hot and dry, while the winter seasons are cold and snowy. However, the pit is located at high altitudes varying from 1710 m. to 1886 m., and that is why the weather conditions are much more severe in the study area compared to Develi center.

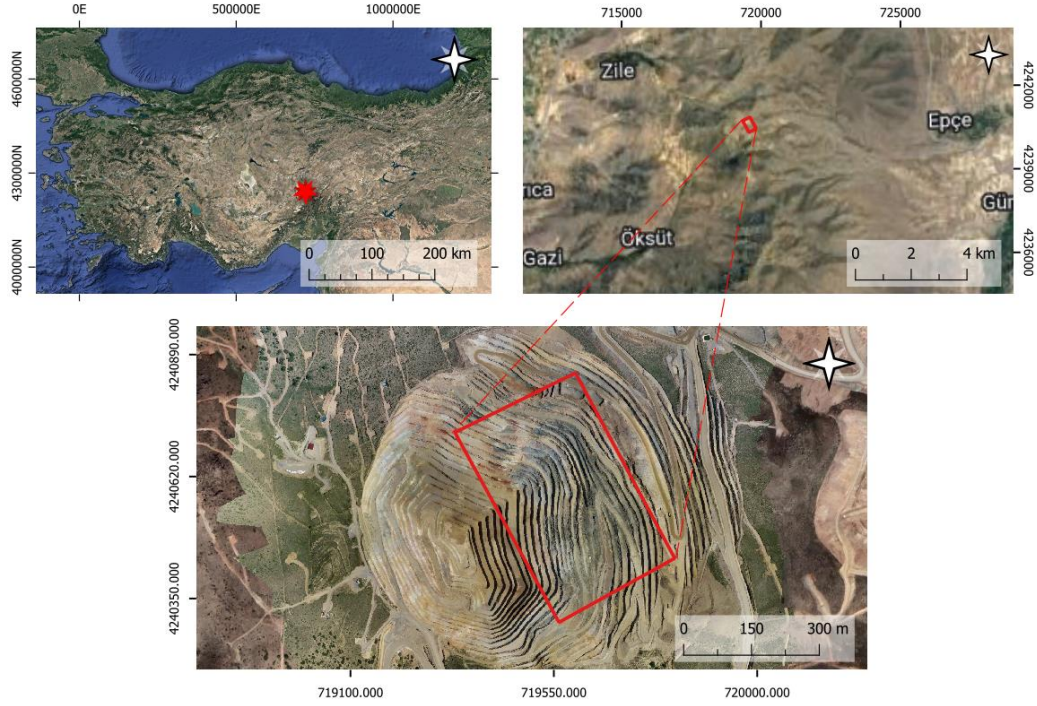


Figure 1.1. Location of study area in the open pit (Kayseri city, Türkiye)

1.3 Geological Background

The Öksüt high sulfidation epithermal gold deposit is present in the Central Anatolian Volcanic Province (CAVP) at the south-eastern piece of the Central Anatolian Crystalline Complex (CACC). Major hydrothermal breccia bodies and hornblende-rich basaltic andesite porphyry, originating from Develidağ Volcanic Complex (DVG) cover the deposit (Aluç et al., 2020).

The alteration and mineralization of Öksüt epithermal gold deposit are present in volcanic and volcanoclastic rocks of the Develidağ Volcanic Center (DVC) at Keltepe mineralized zone. These rocks are composed of different sequences with respect to stratigraphic and compositional characteristics: lower and upper volcanic-volcanoclastic sequences. Although both sequences have the same lithological characteristics, volcanic flow structures and layering exist mostly in the upper sequence. Whereas the lower sequence is composed of basaltic-andesitic flow and dome complex, the lower sequence comprises andesitic to basaltic lava flows hosted conformably by pyroclastic rock on the top (Aluç et al., 2020).

The hornblende rich basaltic andesite (hBA) porphyry and breccias of the lower volcanic-volcanoclastic sequence are the lithologies where alterations occur. The alteration is mainly divided into five types according to the spatial distribution and predominant minerals within the altered rocks: (1) massive silicification to residual silica, (2) quartz-alunite, (3) quartz-alunite ± kaolinite, (4) quartz-kaolinite with alunite ± minor chlorite-smectite and (5) chlorite-smectite (Aluç et al., 2020).

It is known that the Öksüt gold mineralization has an age of 78 ± 32 Ka and is the youngest gold deposit in Türkiye (Aluç et al., 2020).

CHAPTER 2

LITERATURE REVIEW

2.1 Multitemporal analyses with UAVs for change detection

Change detection is a method to identify differences in an object or phenomenon at different epochs (Singh, 1989). This review examines the point cloud comparisons in different studies to understand the change detection process.

Low-cost UAVs systems are very practical and helpful tools in terms of some criteria like time-saving and cost effectiveness to make monitoring an area of interest. However, the evaluation of any data derived from low cost UAVs must be performed before the multitemporal analysis. In this way, the accuracy of the data would be tested as a first phase, and after their reliability would increase for further analyses.

Cook (2017) implemented the evaluation of point cloud data sets derived from his drone by using structure from motion (SfM) in his study. Cook (2017) used a low-cost UAV with placing an independent camera to acquire photographs at a fixed time interval and he made his flights manually. The simple markers made by spray paint on the grounds were used for georeferencing. Cook (2017) separated this study into four main steps to evaluate SfM accuracy based on cloud to cloud comparisons. In the first step, the photograph sets derived from UAV were separated into two groups as odd and even numbers photos by covering the same area with the same ground control points for June 2014 and November 2014 epochs. Then, the point cloud pairs for each June 2014 and November 2014 surveys were compared using the M3C2 algorithm (Lague et al., 2013) in CloudCompare software for reproducibility. In the second step, Cook (2017) used the point clouds derived from LiDAR and UAV to compare in order to assess the distance between two sets of datasets for both June and November 2014 surveys. As a result of these two steps, it was clearly seen that

the differences in the reproducibility phase were closely compatible with the differences in the second phase, and the reproducibility provides a chance to acquire precise estimation if there is no reference dataset like LiDAR scan. In the third phase, the comparison of point cloud datasets from LiDAR and UAV is based separately between the epochs of June and November 2014. Similar change results were obtained in the area of interest. Finally, only UAV-based point clouds were used between the periods of November 2014 and June 2015 to see surface changes. In this study, Cook (2017) showed that the UAV setup is cheap and forms an easy solution to acquire high-resolution topography.

Esposito et al. (2017) focused on the movement of a coastal landslide located in southern Italy for their study. They benefited from photogrammetric processes and SfM algorithm in Agisoft PhotoScan Professional software to generate the point cloud sets, and conducted 3D change detection analysis to monitor the landslide zone effectively. They performed four photogrammetric surveys taking the digital images from a boat and manually using UAV. UAV was used to acquire the images at the cliff toe, and played a complementary role for the data taken from the boat. Then, multitemporal changes were carried out based on the M3C2 method (Lague et al., 2013) by using the point clouds derived from the images taken on the boat and UAV. As a result, they have detected the erosion and deposition zones accurately in a difficult topography like coastal area.

Ahmad Fuad et al. (2018) studied the point cloud datasets derived from mobile laser scanner to find the best point cloud registration method and cloud-to-cloud distance method in CloudCompare software. Two survey epochs were used to perform surface change detection analysis. The researchers benefited from Matching Bounding Box Centers (MBBC) and Iterative Closest Point (ICP) methods for point cloud registration, while they used four main cloud-to-cloud distance methods; for instance, nearest neighbor, least square plane, quadric, 2.5D triangulation to analyze surface deviation. In the meantime, the UAV data were collected from the site to compare two types of datasets using the same methods. According to the comparison of surface deviation values, it was clearly seen that ICP registration method and Least

Square Plane (LSP) provided better results than the other methods by using the data from mobile laser scanner, and the data from UAV gave the similar results with the laser scanner data under the change detection analysis.

Hayakawa & Obanawa (2020) performed their study in bedrock cliffs of a coastal island in Japan to detect the changes on bedrock. For this, terrestrial laser scanning (TLS) and unmanned aerial system (UAS) were used for 5 years in the study. The repetitive surveys were conducted with TLS, and iterative closest point (ICP) technique was used to align the data from derived from TLS. These data were used to align UAS-based point clouds. 3D mesh polygons were produced by using the point clouds derived from UAS which have high accuracy position. The temporal 3D meshes enable researcher to identify the changes in the cliffs during the study time. In conclusion, Hayakawa & Obanawa (2020) observed morphological changes and enables them to estimate the average erosion volume per month at the end of the study.

Kyriou et al. (2022) conducted a study in Northern Peloponnese, one of the most tectonically active region in the world. The purpose of the study is to monitor a landslide in a steep valley by acquiring multitemporal data by UAV and TLS survey and to inform the local authorities about the stability of the area of interest. The direct-to-direct comparison detected the surface changes in multitemporal point clouds derived from both RADAR and TLS. This also enables Kyriou et al. (2022) to compare both types of datasets, and it was concluded that the evolution of landslide might be assessed with TLS-based point sets more accurate than UAV. In addition, small scale displacements obtained by TLS results were verified by GNSS measurements. Kyriou et al. (2022) suggested that the integration of UAV and TLS increases efficiency for monitoring and fast detection of deformations.

Teo et al. (2023) performed their study in the Wuhe landslide in Taiwan. The purpose of the researchers to acquire displacement fields in major landslide mapping by using UAV photogrammetry. The researchers used DJI Phantom 4 RTK to increase the absolute accuracy with low number of ground control points, and they acquired three

data types such as orthomosaic, digital surface model and point cloud for two epochs. The main purpose is to consider three different techniques using UAV photogrammetry, and to observe the landslide displacement with respect to these techniques. In order to obtain 2D and 3D displacement fields, image-based PIV, DSM-based PIV and Point-based ICP are used, and the efficiency of each of them is evaluated. The researchers concluded that the point-based ICP gives better results than the others, and it can be used as an alternative data to LiDAR point cloud for obtaining 3D displacements and angular changes.

2.2 Multicriteria Analysis in GIS Environment

Multi-criteria Decision Making (MCDM) is one of the correct and revolutionary methods (Taherdoost & Madanchian, 2023), and it is developed by Benjamin Franklin based on his study on moral algebra (Hajduk, 2022). This method is also used to create landslide susceptibility mapping and acquire a single-composite resultant with several parameters (Malczewski, 1999).

There are some multicriteria decision methods used in the GIS environment. These are the weighted linear combination (WLC) which is commonly used GIS environment for multicriteria analyses (Malczewski, 2000), the analytic hierarchy process (AHP) (Saaty, 1987), the ordered weighted average (OWA) (Yager, 1988). In this review, AHP methods will be examined with some researches.

Yeon et al. (2010) conducted a study in a rocky mountainous area which was affected by landslides due to heavy rainfall in Korea. Thus, a landslide susceptibility map was created using a decision tree, one of the famous classification algorithms. Thirteen input attribute layers are extracted from the landslide location map, topographic map, soil map and forest map to acquire landslide susceptibility map. The researchers concluded that a decision tree is an efficient method for spatial prediction issues.

Feizizadeh & Blaschke (2013) created landslide susceptibility mapping by various multicriteria decision analysis methods around the Urmia lake basin. These methods

are analytic hierarchy process, ordered weighted average and weighted linear combination respectively. The researchers tried to find the best method by using the existing landslide dataset and compare them with each landslide susceptibility map derived from three methods. As conclusion, the AHP method provides better results than OAW and WLC methods.

Basharat et al. (2016) performed landslide susceptibility analysis around NW Himalayas in Pakistan. Nine factors were taken into consideration, and weights of the factors were acquired with pairwise comparison in AHP. Then, the susceptibility map was produced by using a weighted overlay method in GIS. The landslide occurrence is used to verify the obtained susceptibility mapping, the verification results showed 76% accuracy which represents a good accordance between susceptibility map and landslide occurrence.

El Jazouli et al. (2019) conducted a study in the high Oum Er Rbia River basin in the Middle Atlas Mountain region where landslide issues often occur. El Jazouli et al. (2019) created a landslide susceptibility map (LSM) with eight factors by using AHP method. LSM was divided into five classes based on the natural break method. As a result of the study, LSM contributed to obtaining information about the landslides which occur today and might occur in future, and it is found that it is very useful for decision makers to prevent landslide risks.

Devara et al. (2021) performed GIS-based multi-criteria analysis to create landslide susceptibility map by using multi-temporal interferometric synthetic aperture radar (MT-InSAR) as an input parameter. AHP method was used to form multi-criteria analysis with seven factors in the study. ERS1/2 & Envisat and Sentinel-1A were used to interpolate the deformation values in the study area and they were used in reclassification as well as DEM-derived products, lithology, geomorphology, land use/land cover (LULC) maps to detect landslide susceptible zones. Devara et al. (2021) compares landslide susceptibility maps (LSM) including MT-InSAR and not including MT-InSAR to assess contribution of MT-InSAR to the preparation of

LSM. In conclusion, utilizing MT-InSAR as a parameter improved the creation of landslide susceptibility map.

Bhagya et al. (2023) conducted their study on landslide around Western Ghats. The researchers aim to evaluate landslide susceptibility of area of interest with AHP and fuzzy-AHP models, the performance of these two models with present landslide susceptibility maps. Ten factors are used, and the landslide susceptibility zones were divided into three categories as low, moderate, and high. The receiver operating characteristic (ROC) technique is used to evaluate the efficiency of the AHP and F-AHP map. As a result of spatial analysis, the maps using Tool for Infinite Slope Stability Analysis (TISSA), fuzzy-AHP (F-AHP) and AHP have very good performance with AUC values which are above 0.80.

CHAPTER 3

METHODOLOGY

The methodology of the study comprises five main stages. The stages are preparation of flight path, selection of ground control points, photogrammetric processes, data analysis and instability assessment mapping (Figure 3.1). Individual phases are explained with details below.

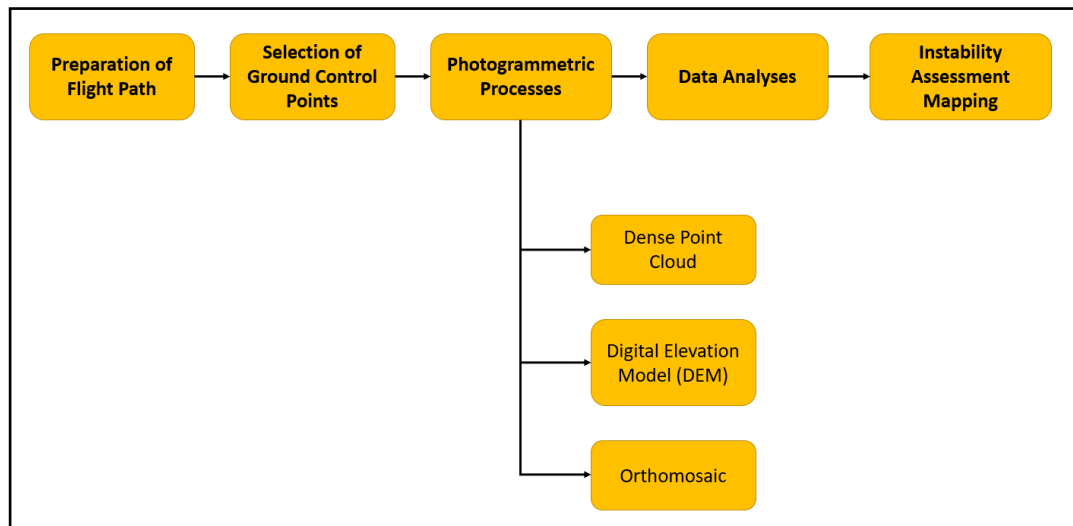


Figure 3.1. The methodology of the study.

3.1 Preparation of Flight Path

A flight path is firstly prepared to take airborne photos of the selected area of the East pit in “DJI Terra” software (Figure 3.2). The starting point is arranged as the closest point to home point in order to complete the flight route with a single battery. Estimated flight route time is approximately 26 minutes for a flight route distance of

7248 meters with a flight altitude of 30 meters. The side and forward overlap ratios are chosen as 60 percent producing 627 photos with GPS assisted coordinates.



Figure 3.2. Flight path for the target zone in “DJI Terra” software.

3.2 Selection of Ground Control Points (GCPs)

Six prisms, which have already installed on the benches for monitoring purposes which do not show any movement or negligible displacement are used as ground control points (Figure 3.3). The already available prisms are chosen for georeferencing processes as placing new stable markers on the benches pose a high risk for health and safety such as any rock failures. Furthermore, the maintenance of new markers requires regular cleaning up due to the presence of continuous dust or other weather effects on the site, which would also increase the exposure of workers to hazards.

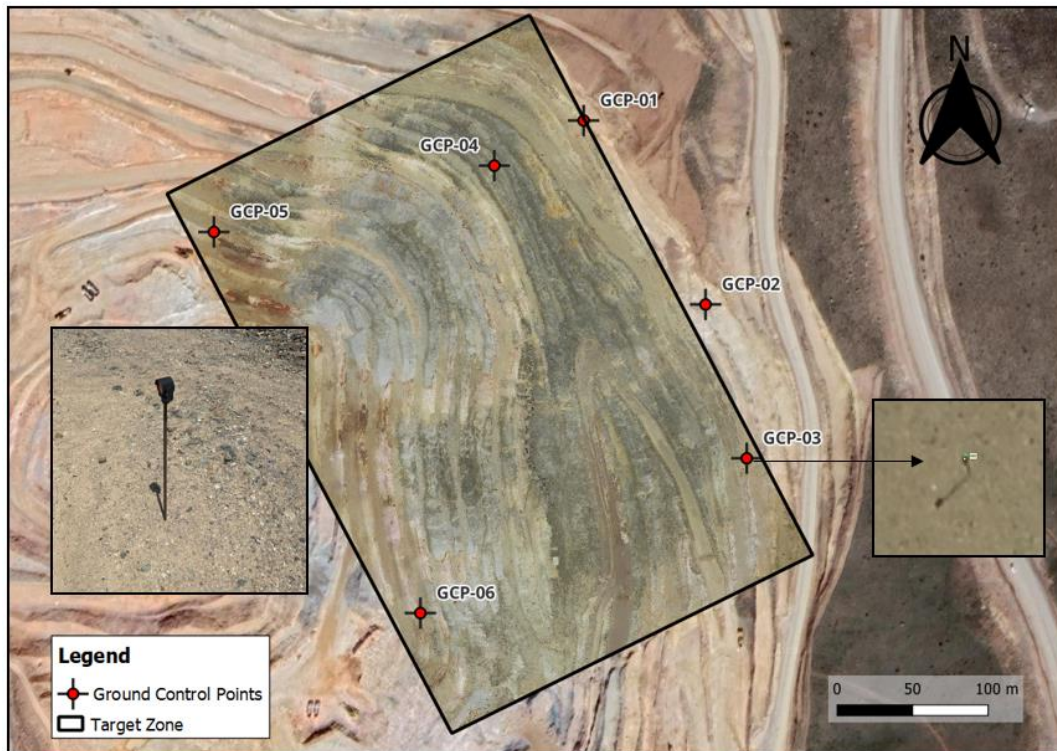


Figure 3.3. Ground Control Points in the study area.

3.3 Photogrammetric Processes

In this study, five survey processes are conducted in a licensed Agisoft Metashape professional v2.0 software (*Agisoft Metashape User Manual Professional Edition, Version 2.0, 2023*) to acquire necessary data such as point cloud, digital elevation model, and orthomosaic. The initial survey is performed 08/09/2022, and this date is accepted as a reference in time scale to make related evaluation of change detection analysis and to create an instability assessment map.

All of the survey data are created in Agisoft Metashape professional v2.0 software (*Agisoft Metashape User Manual Professional Edition, Version 2.0, 2023*), and processes in this software are basically divided into three phases. In the first phase,

an alignment process which contains aerial triangulation and bundle block adjustment is performed to enable the software to detect feature points on the images, and to provide a relationship between images and tie points. After the alignment process, ground control points can be marked for the images containing the markers, and dense point clouds can be built up. In the second phase, the user can create a mesh or digital elevation model (DEM) by using the generated dense point cloud. Finally, the orthomosaic may be generated if desired.

A snapshot of the application windows with possible parameters is presented in Figure 3.4. In this study, the quality of these data is selected high, and the other options are left as default. As a result of the procedures, the dense point clouds, digital elevation models, and orthomosaics are obtained for each survey (Figure 3.5). Acquisition dates and ancillary information of photogrammetric sets are presented in table 3.1.

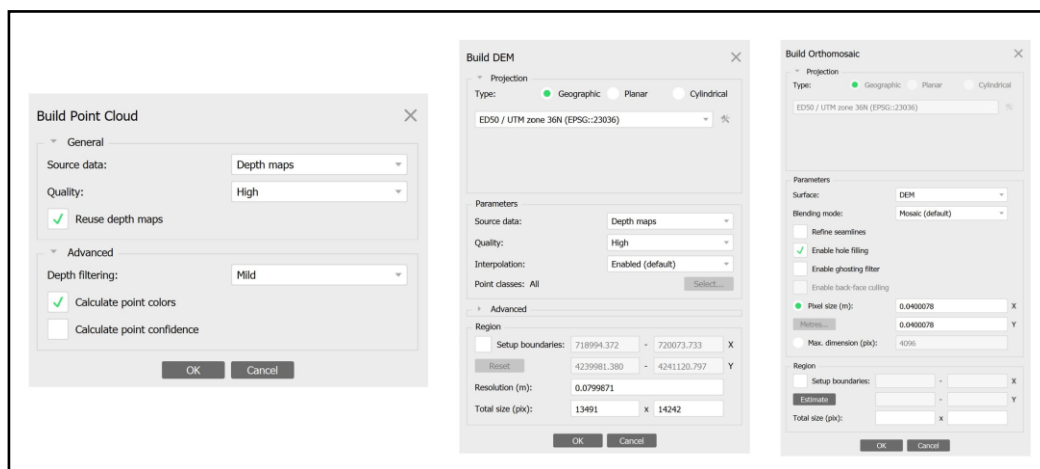


Figure 3.4. The parameters that represent the processes of the generation of point cloud, DEM and orthomosaic in the Agisoft Metashape interface.

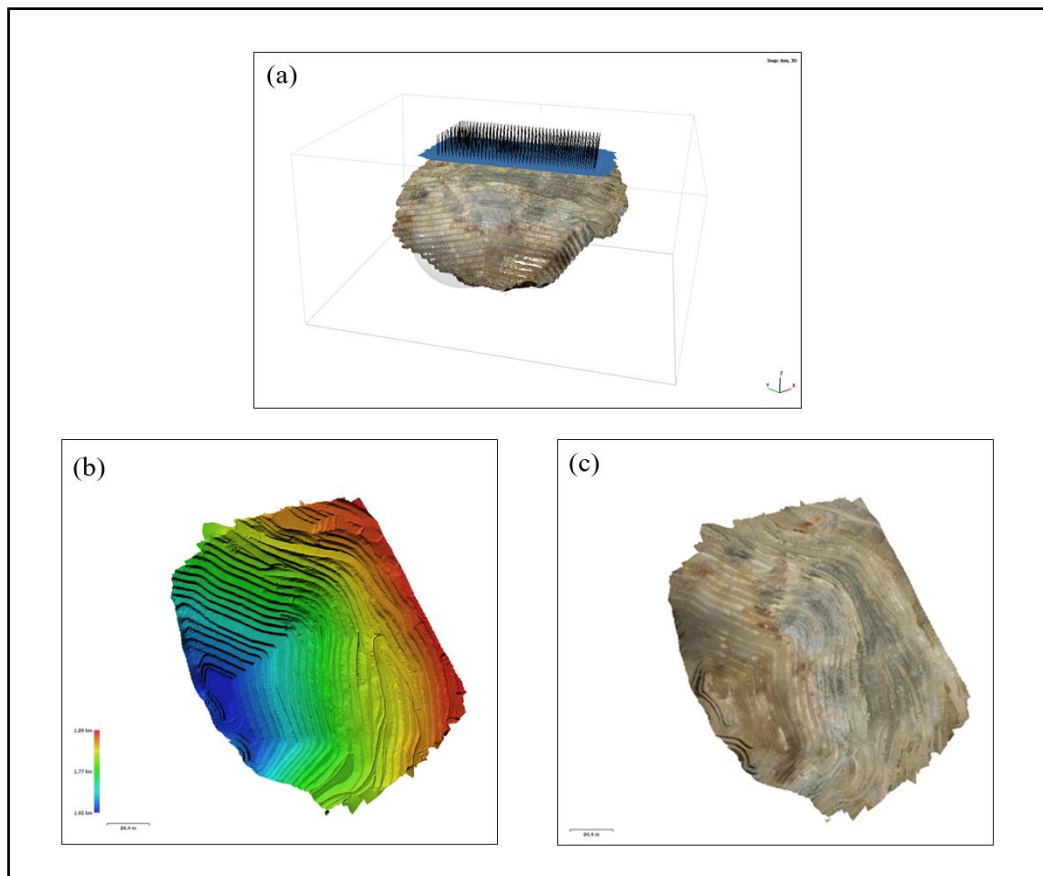


Figure 3.5. a) The dense point cloud, b) Digital Elevation Model, c) Orthomosaic generated in Agisoft Metashape Professional software.

Table 3.1 Summary information of each survey data

Date	<i>08/09 2022</i>	<i>19/12 2022</i>	<i>24/01 2023</i>	<i>07/03 2023</i>	<i>26/06 2023</i>
Number of Images	549	549	549	549	549
Flying Altitude	143	143	143	143	143
Focal Length (mm)	8.8	8.8	8.8	8.8	8.8
Ground Resolution (cm/pix)	4.3	4.26	4.32	4.27	4.3
Coverage area (km²)	0.108	0.108	0.108	0.108	0.108
Number of GCP s	6	6	6	6	6
X error (cm)	0.670	0.736	0.478	0.871	0.800
Y error (cm)	0.643	0.710	0.674	0.688	0.786
Z error (cm)	0.643	1.058	0.829	0.554	0.4780
XY error (cm)	0.929	1.023	0.826	1.110	1.122
Total (cm)	1.438	1.472	1.171	1.241	1.220
Error (pix)	0.354	0.386	0.364	0.405	0.362
Point Cloud	12,624,379	16,211,820	14,637,639	13,547,434	12,891,827
DEM resolution (cm/pix)	8.0	8.0	8.0	8.0	8.0
Orthomosaic resolution (cm/pix)	4.0	4.0	4.0	4.0	4.0

3.4 Data Analyses

The data analysis part is mainly divided into six phases (Figure 3.6). In the first phase, change detection analyses are performed by using point cloud (derived from UAV) comparisons in CloudCompare software to detect the failure locations with the zone of accumulated material. In the second phase, the photogrammetry-based data is compared with the relative range data obtained by the SSR in the mine site to observe the accuracy of the photogrammetry data. In the third phase, the alteration types are assessed in terms of stability. The volumes of the accumulated material on the benches are calculated in the fourth part. The fifth phase explores tension crack

mapping and the connection between the cracks and stability are explored. Finally, creation of slope map is shown in detail.

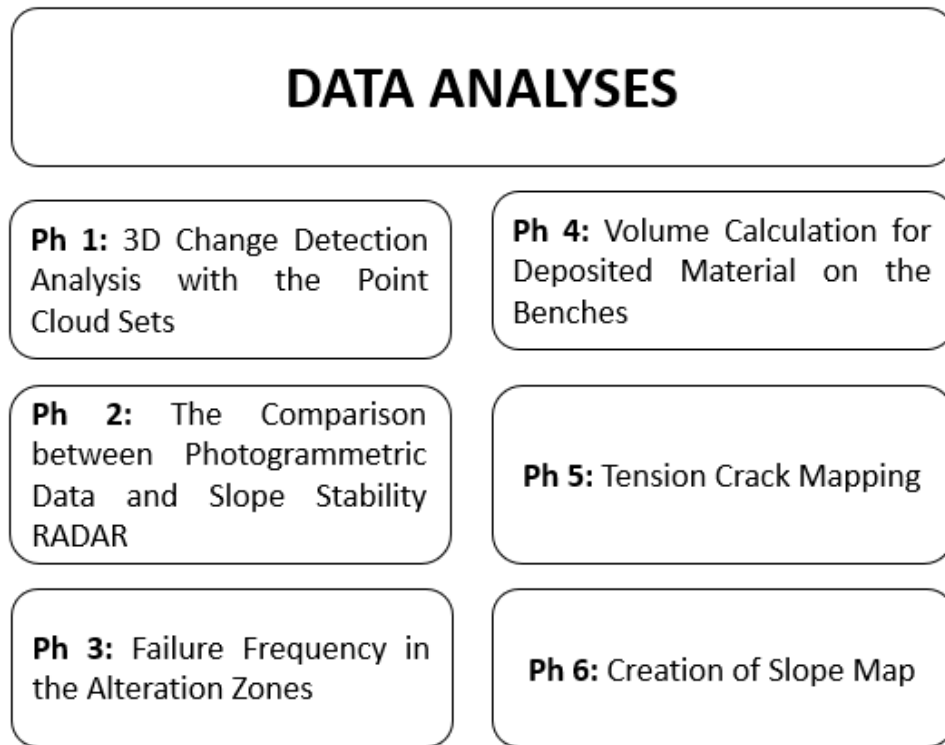


Figure 3.6. The phases of the data analyses

3.4.1 3D Change Detection Analysis with the Point Cloud Sets

Five point cloud datasets derived from UAV are used to make change detection analysis with multiscale model-to-model cloud comparison (M3C2) method (Lague et al., 2013) in CloudCompare, a free software. First step is cloud registration tool to align each point cloud derived from UAV finely. The point cloud data taken in September 08, 2022 is selected as the reference epoch for each comparison to observe all the changes in 3D view on the pit during ten months. Second step is

M3C2 distance calculation for point cloud data sets by using the M3C2 algorithm to compute vertical normals. The parameters of normal scale diameter and projection scale diameter are provided by the help of “guess params” option within the software. As a conclusion, normal diameter is 0.92 m and projection diameter is 1.86 m are determined and “cloud #1” is selected as core points during the normal calculations process for each point cloud datasets. All of the results are shown in figures 3.7, 3.8, 3.9 and 3.10. Red represents the bench scale failures while blue shows the accumulated material on the benches, and red dash lines shows the displacement caused by operational process (Figure 3.10). In failure parts, the min value is -2.41m that represents max displacement and average value is -0.03 meters.

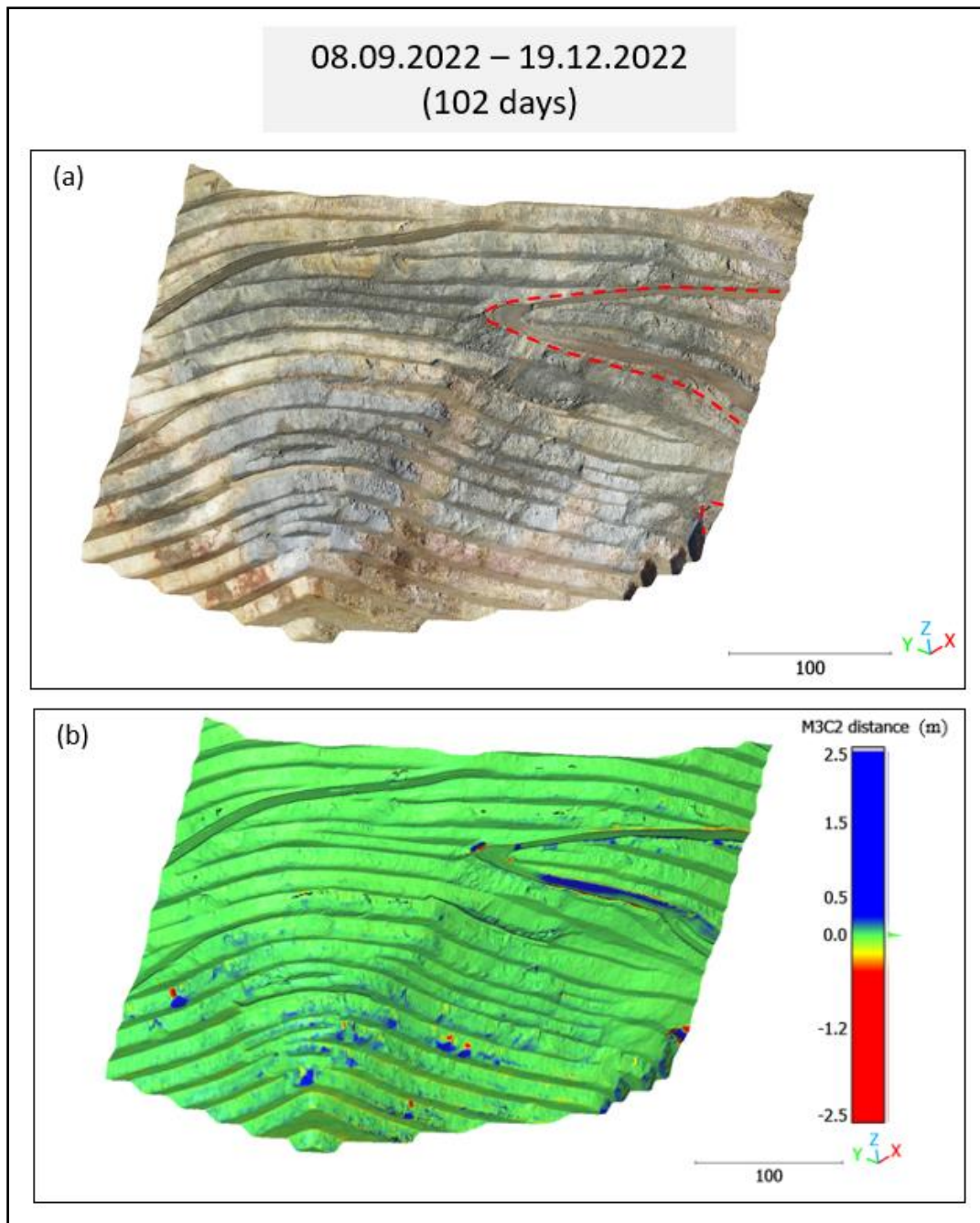


Figure 3.7. a) Colored-point dense cloud for 19.12.2022 (red dash lines represent the displacement caused by operational process). b) 3D change detection with M3C2 method in the dates between 08.09.2022-19.12.2022

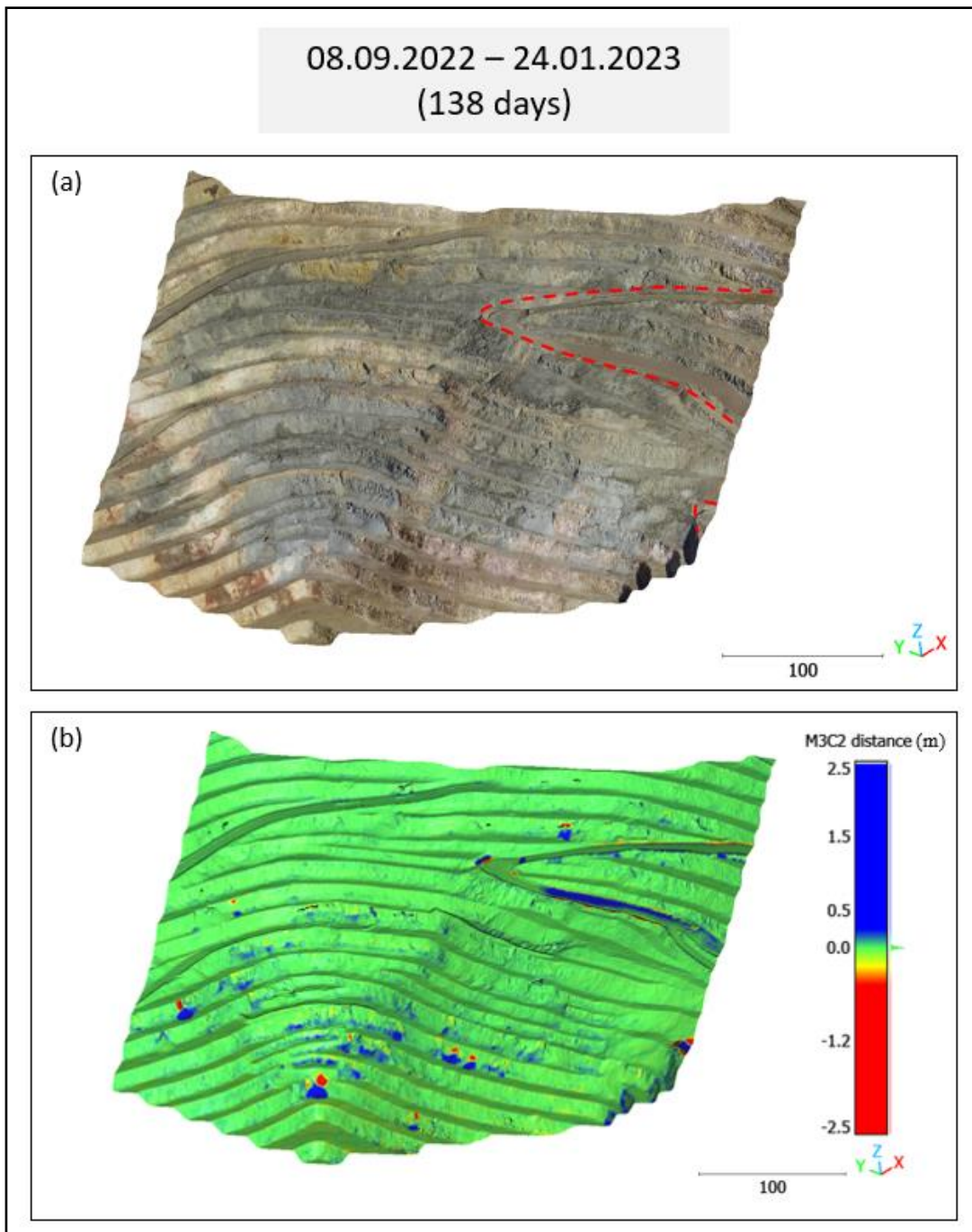


Figure 3.8. a) Colored-point dense cloud for 24.01.2023. (red dash lines represent the displacement caused by operational process). b) 3D change detection with M3C2 method in the dates between 08.09.2022-24.01.2023

08.09.2022 – 07.03.2023
(180 days)

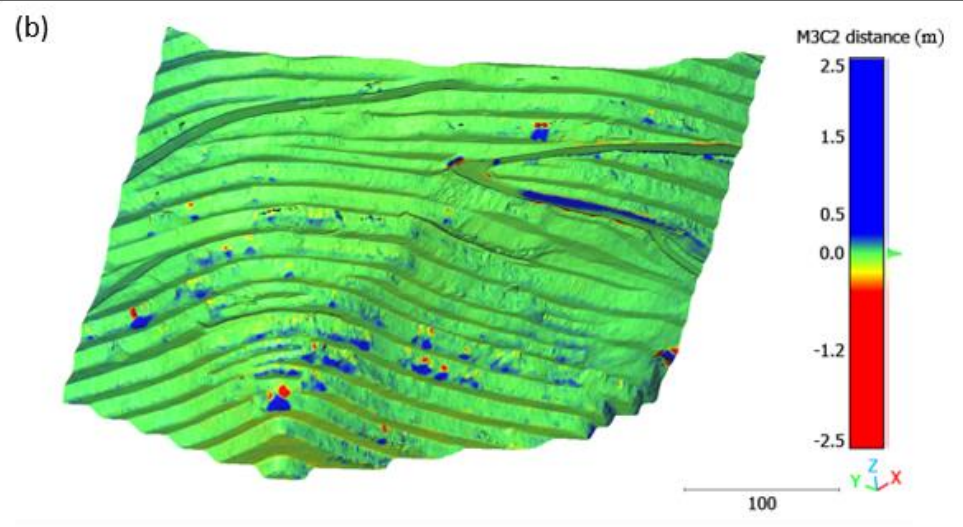


Figure 3.9. a) Colored-point dense cloud for 07.03.2023 (red dash lines represent the displacement caused by operational process). b) 3D change detection with M3C2 method in the dates between 08.09.2022-07.03.2023

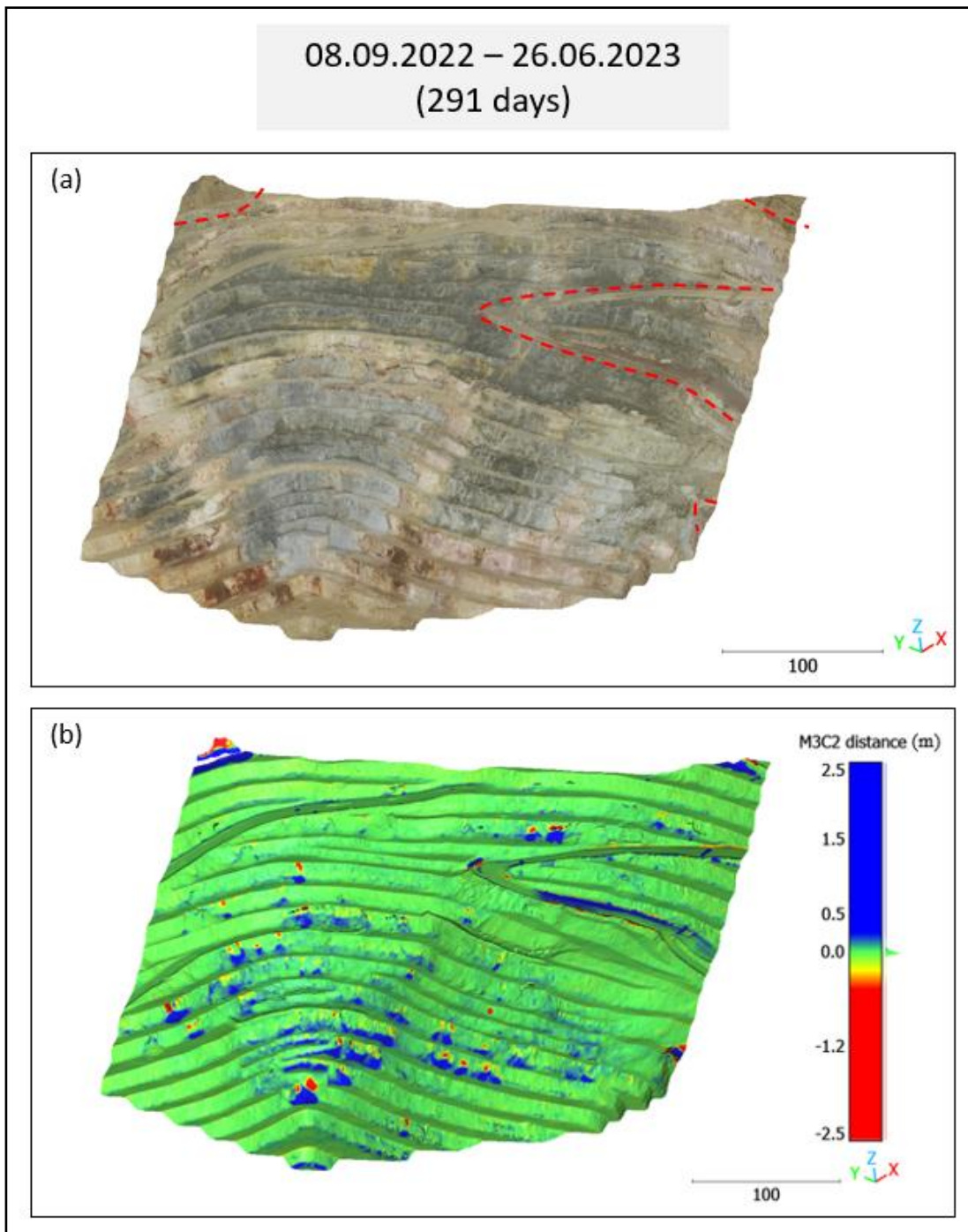


Figure 3.10. a) Colored-point dense cloud for 26.06.2023 (red dash lines represent the displacement caused by operational process). b) 3D change detection with M3C2 method in the dates between 08.09.2022-26.06.2023

3.4.2 The Comparison between Photogrammetric Data and SSR Data

The point cloud comparison is an effective methodology to analyze the changes in the study area. In this study, other monitoring data is used to observe the differences and similarities between photogrammetric data and selected monitoring tool. That is why SSR data is included to compare the M3C2 distance values obtained from the point cloud data sets by UAV and relative range values by SSR. Firstly, small-scale failures are observed on the point cloud data derived from UAV of M3C2 distance (m) calculation (Figure 3.11-a). Secondly, the point cloud data derived from SSR is checked to compare both data sets (Figure 3.11-b), and it is realized that the deformation zones are compatible with drone and SSR-based data. Four certain deformation zones are detected and indicated by red dash lines on the image-draped point cloud of last epoch (Figure 3.11-c). In other words, the overall situation indicates that these tools provide similar results to detect the failure locations with the frequency and magnitude. For further analyses, a series of profiles and swath profiles are created in this section.

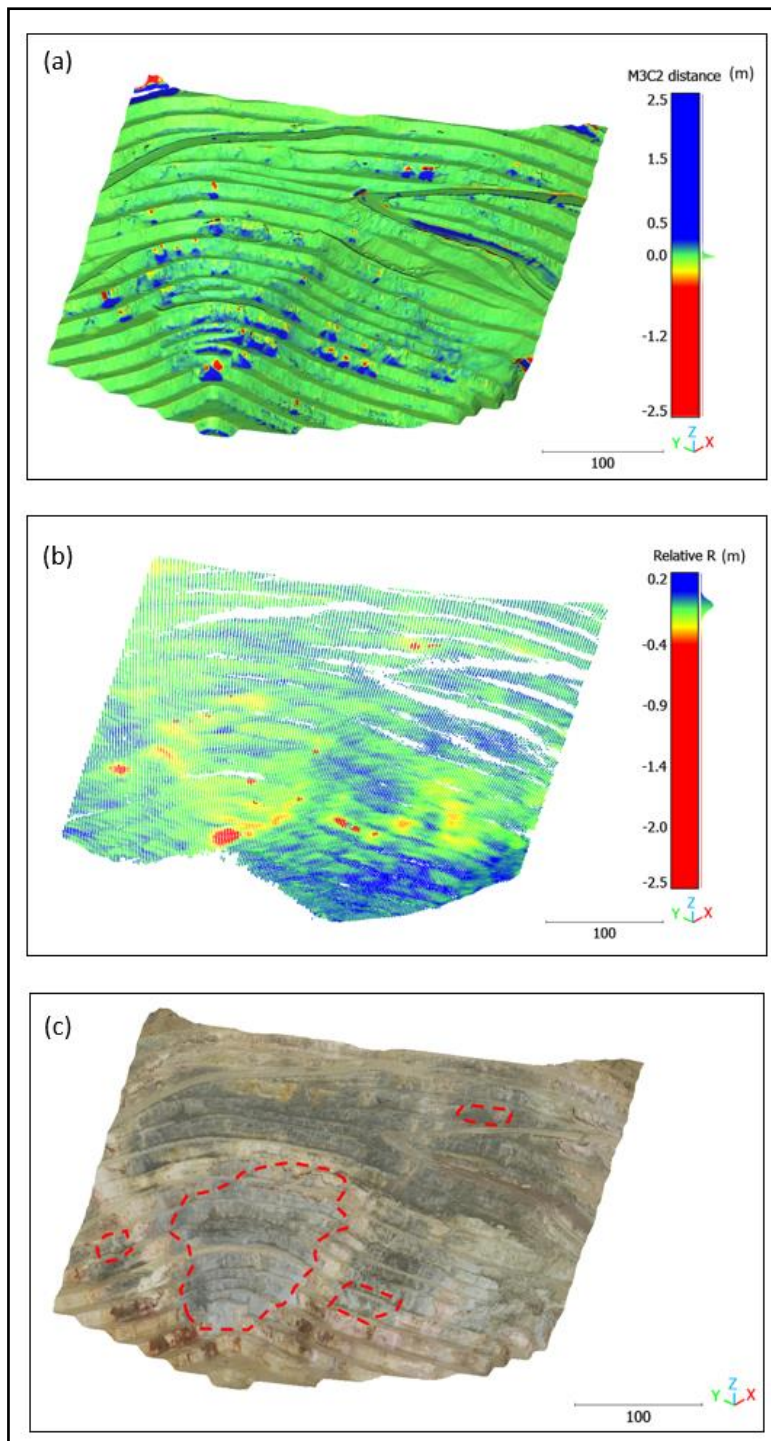


Figure 3.11. a) Point cloud data of M3C2 distance method in between 08/09/2022 and 26/06/2023. b) Point cloud data (relative range) of SSR in between 08/09/2022 and 26/06/2023. c) The image draped point cloud data in 26/06/2023 and red dash lines represent the regions where small-scale failures occurred.

The point cloud datasets from SSR and photogrammetry are first imported in QGIS software to compare them in detail. The next step is to transform point clouds into the raster data by using *TIN interpolation* (Figure 3.12). Finally, a profile line is drawn passing through areas where most bench-scale failures are observed and a profile A-B is plotted with *Profile Tool* to check the compatibility of SSR and photogrammetric data (Figure 3.13). When eleven failure locations are examined, the movement values of both raster types provide very similar results and range from -0.3m to -2m. However, in the parts of the accumulation of materials, the values do not converge to each other which means that Drone based image photogrammetry is a much more successful monitoring tool to detect the location of accumulated material on the benches than SSR-relative range precisely. The same situation is clearly seen with four longitudinal profile lines (Figure 3.14, 3.15 & 3.16).

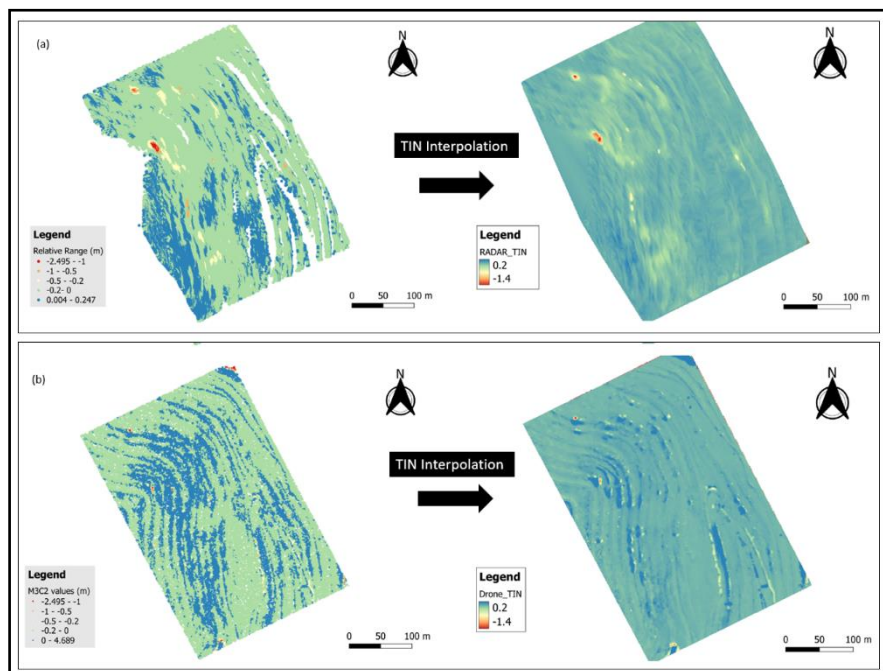


Figure 3.12. a) The relative range data of SSR and the transformation of point cloud data to raster data by using TIN interpolation. b) M3C2 distance data and the transformation of point cloud data to raster data by using TIN interpolation.

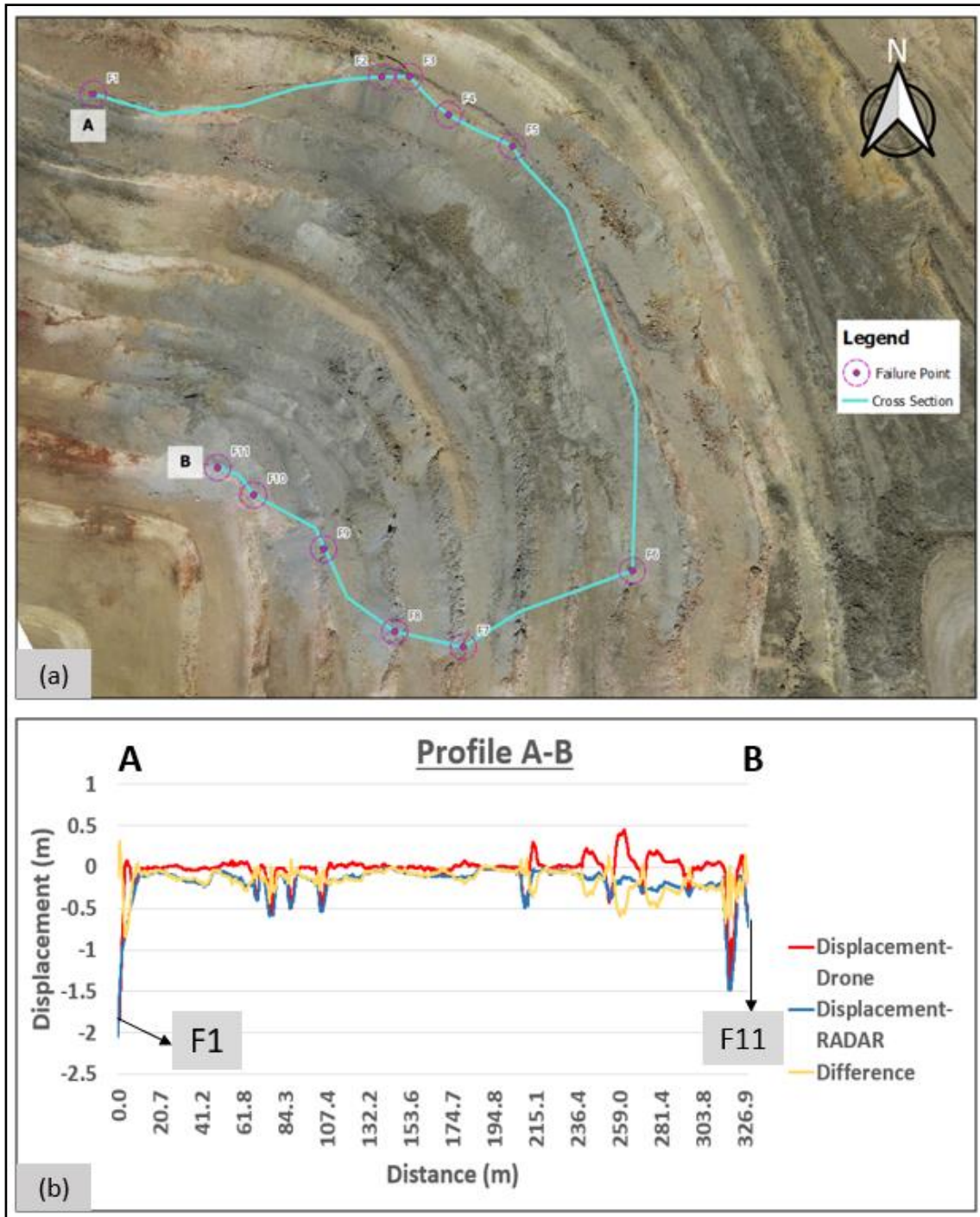


Figure 3.13. a) The line of profile A-B on the map. b) The profile A-B.

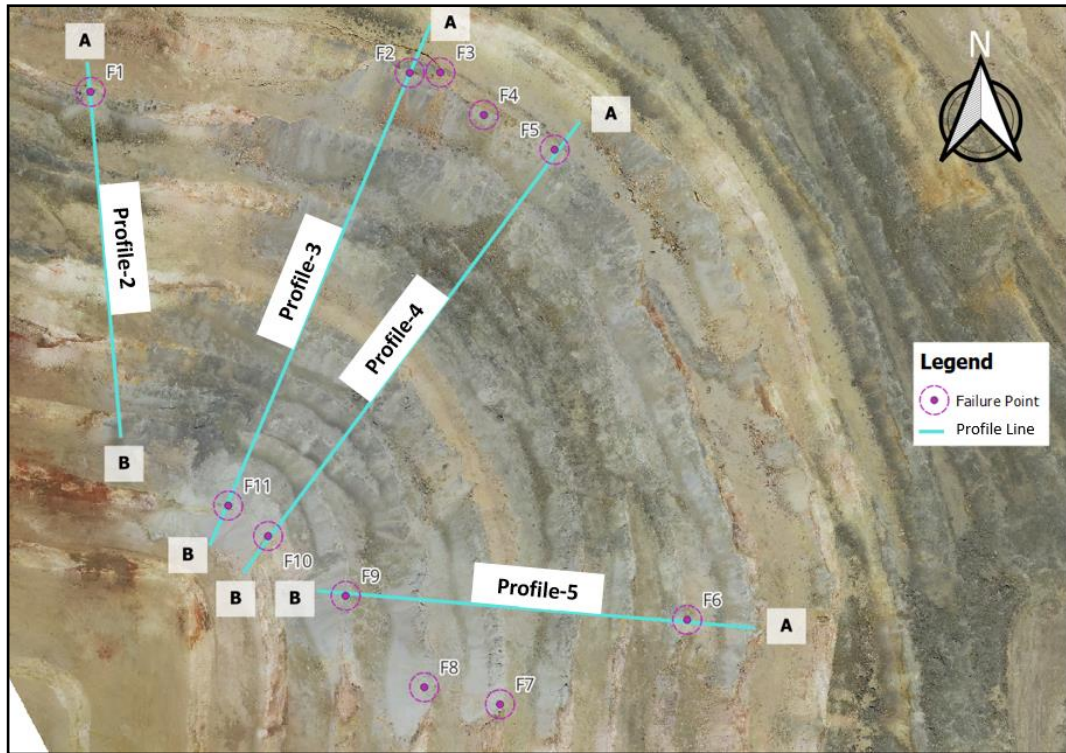


Figure 3.14. The longitudinal profile lines on the map

The argillic zone as shown in figure 3.17 is the area that the most of the bench scale failures are abundant. Therefore, it is quite a suitable section to evaluate in terms of statistics. The number of the point clouds of SSR and drone are 17116 and 33932 in the target zone. After filtering movement values above 0 m, movement histograms are created for both types of monitoring tools to compare. The histogram graphs show that the values are concentrated between 0 m and -0.2 m which represents slight material movement while the distribution of the values below -0.2 m indicate small-scale failures on the slopes and benches. The accordance of two histogram plots are good enough to evaluate the general situation and the variations are caused by the different number of points and the differences in the sensitivity of the tools. However, it does not change the overall situation of the small failures. In addition to that, a swath profile line is defined through 140 meters covering the argillic zone totally with 70 profile lines (Figure 3.18-a). Afterwards, the profiles are created to

show the minimum, maximum and mean displacement values from both SSR and Drone data (Figure 3.18-b & Figure 3.18-c). According to the swath profiles, the photogrammetric data is compatible with SSR data for the value below 0 m which represents the bench-scale failures. On the other hand, an incompatibility is found in the displacement values above 0 m which shows the location of the material accumulation. As a result of the profiles and swath profiles, the material accumulation on the benches is detected effectively with UAV rather than SSR, and UAV monitoring is applied successfully just like SSR to see all failures in the mine site.

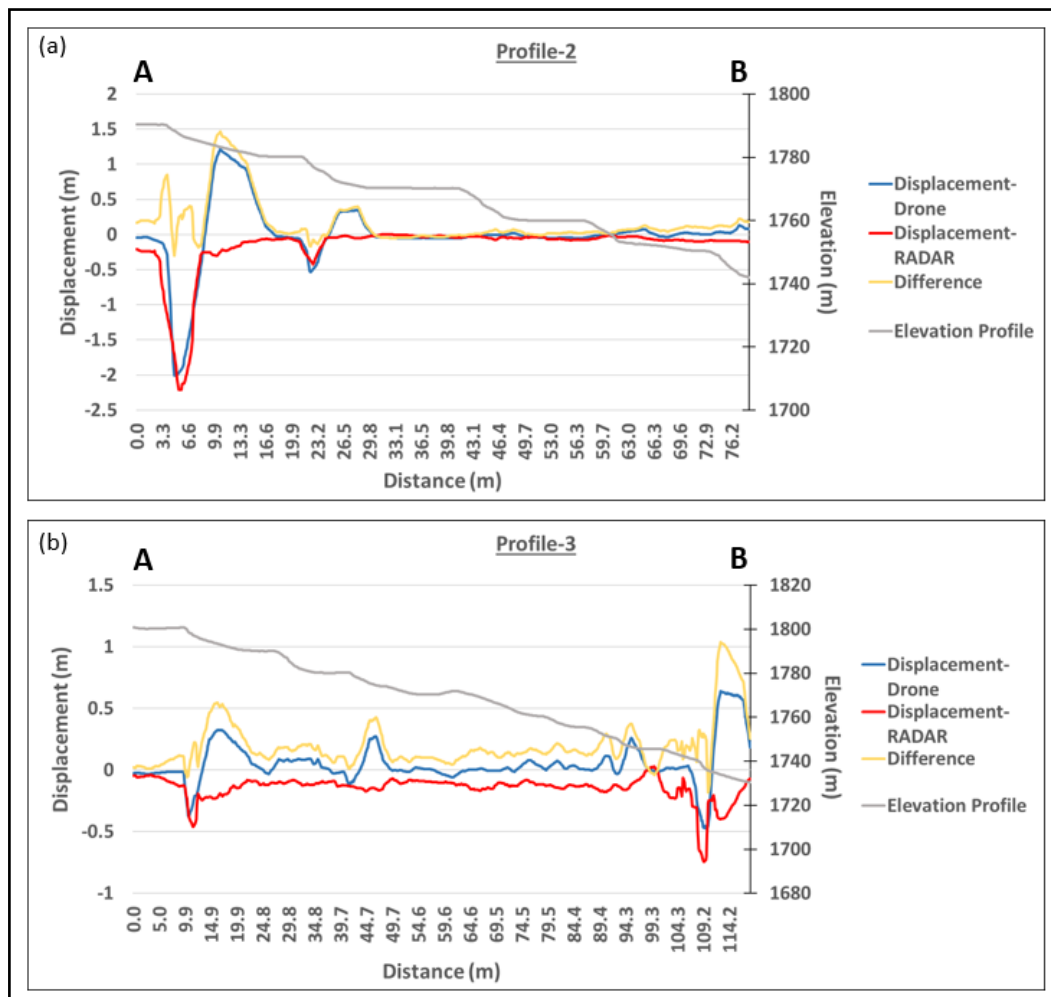


Figure 3.15. (a) Displacement graph of profile 1, (b) profile 2.

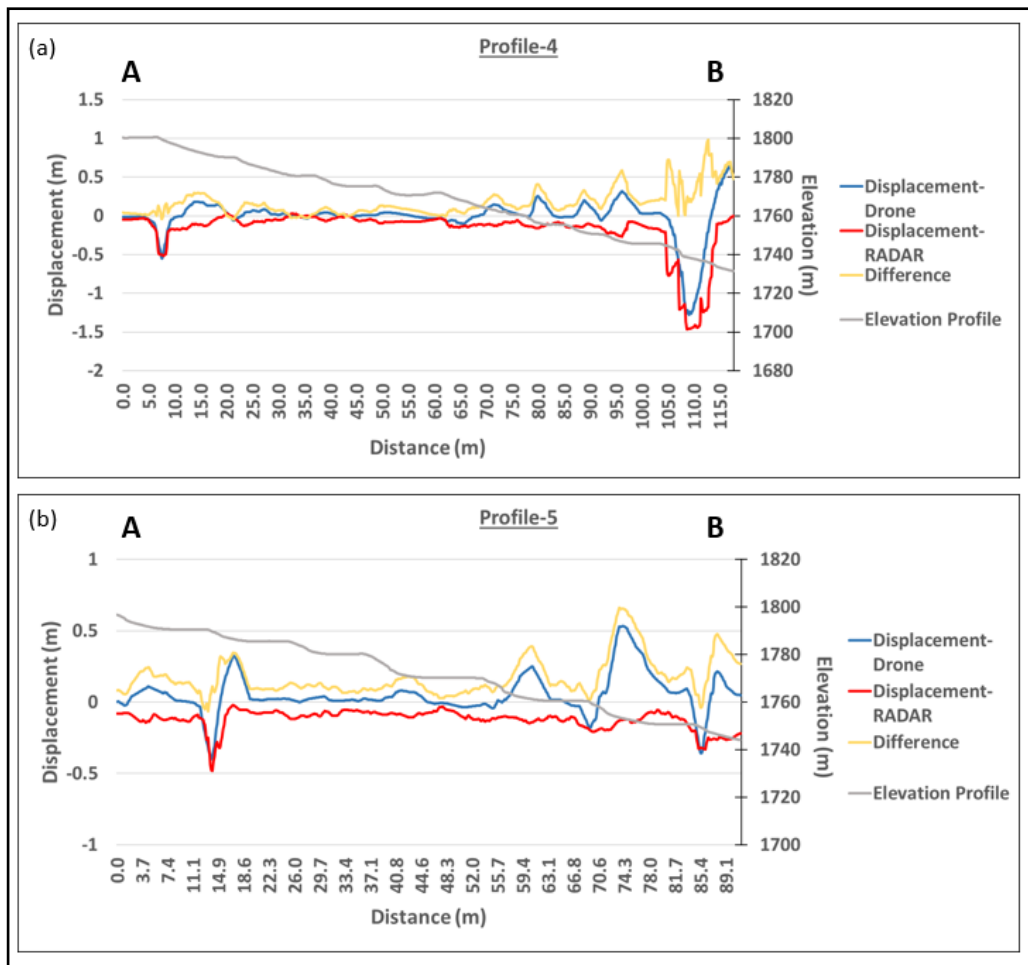


Figure 3.16. (a) Displacement graph of profile 3, (b) profile 4.

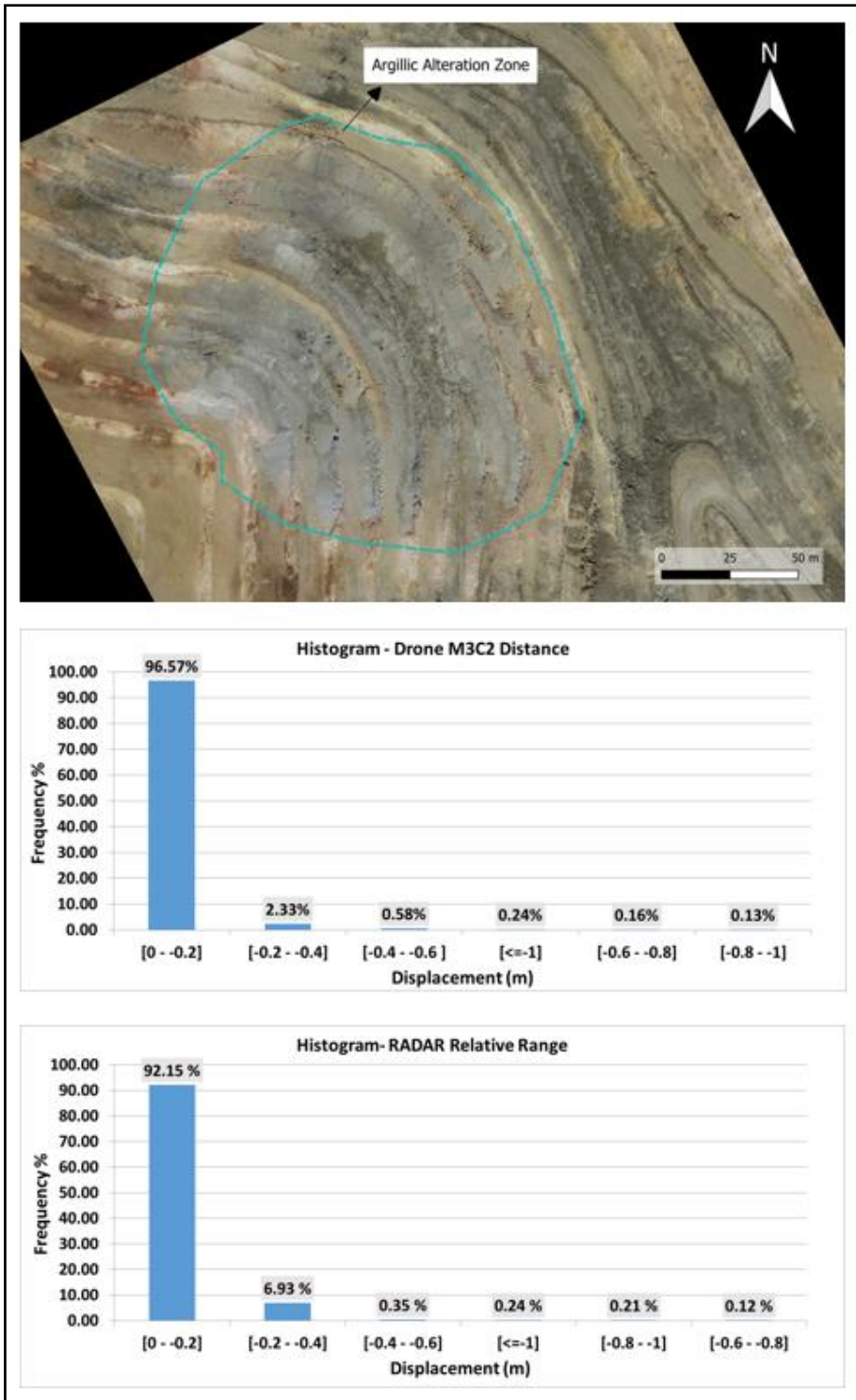


Figure 3.17. Histograms of SSR and photogrammetric data based on the percentage of point cloud data which represents the failure points in the argillic alteration zone.

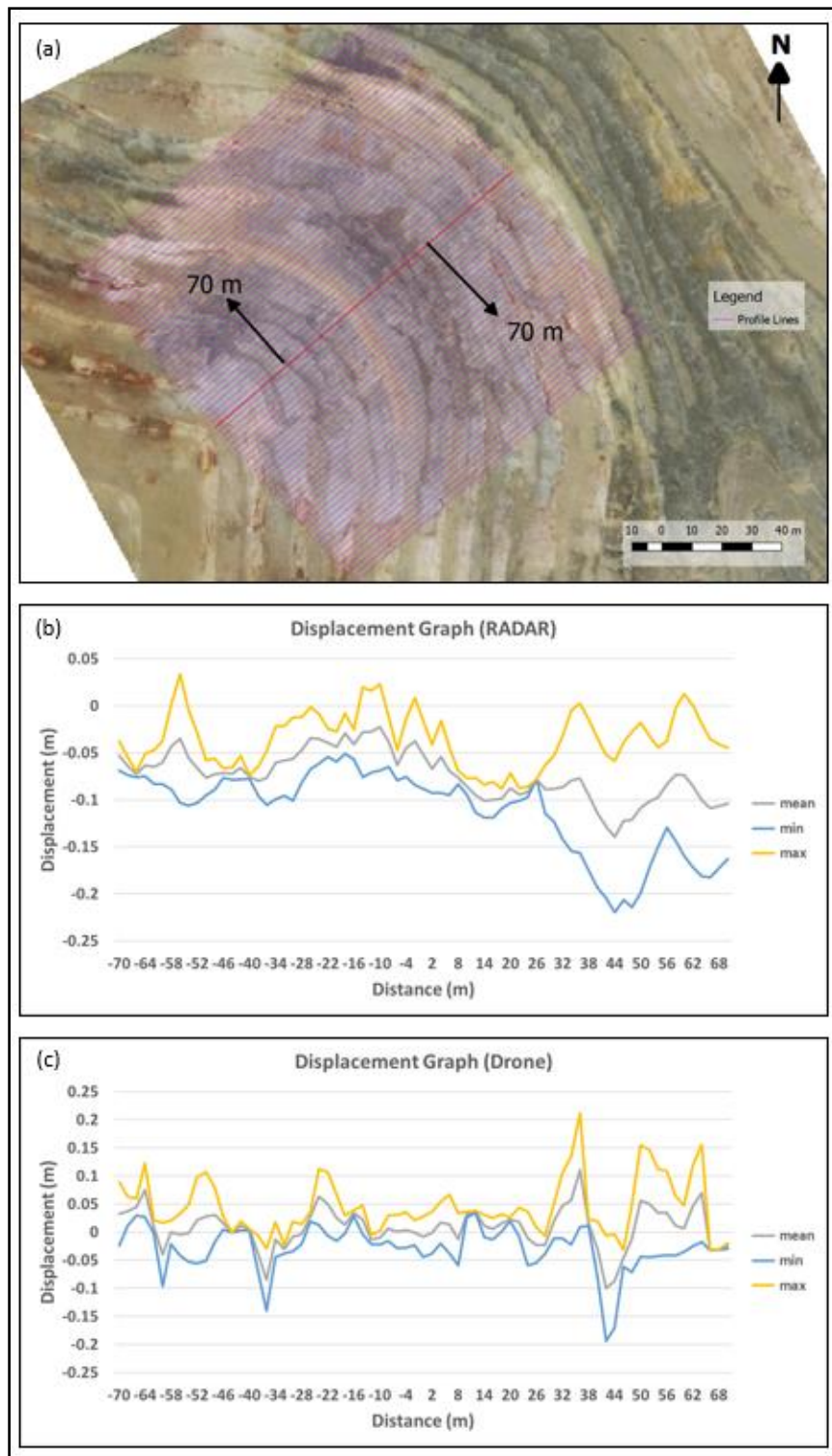


Figure 3.18. a) The location of the profile line used in the swath profile on the map, b) the swath profile of SSR based data (08/09/2022-26/06/2023), c) the swath profile of Drone based data (08/09/2022-26/06/2023).

3.4.3 Failure Frequency in the Alteration Zones

The alteration types in the pit play an important role in the stability. Thus, the alteration types are crucial to find the relationships between alterations and failures location. Firstly, elevation differences are calculated by using *raster calculator* with DEM data of all epochs in QGIS, and the resultant difference data is vectorized where only negative elevation values are filtered to acquire the failure polygons (Figure 3.19). Secondly, the filtered failure polygons are converted into centroid points, and are presented on the map (Figure 3.20). In order to understand the effects of alteration to the failure density, the alteration map which is digitized in QGIS by using the georeferenced map acquired by mine geology team (Figure 3.21) is overlain and centroids of the failures are count automatically using *count points in polygons* options in QGIS. The failure distribution is shown on the graph for each time interval (Figure 3.22). According to the results, the alterations can be ordered Arg-Type1, Arg-Type2, QKao, QAIK, QAI and MS from most unstable to less unstable alteration types. The argillic alteration is divided into two section as type-1 and type-2 because weathering effects are dominant in Arg-type1, the graph in figure 3.22 also prove this situation. Figure 3.23 shows the limits of the argillic alteration type 1 and the failure points of last epoch with existing tension cracks. As a result, the argillic alteration type-1 (Arg-Type1) is the worst alteration type in terms of stability in the pit.

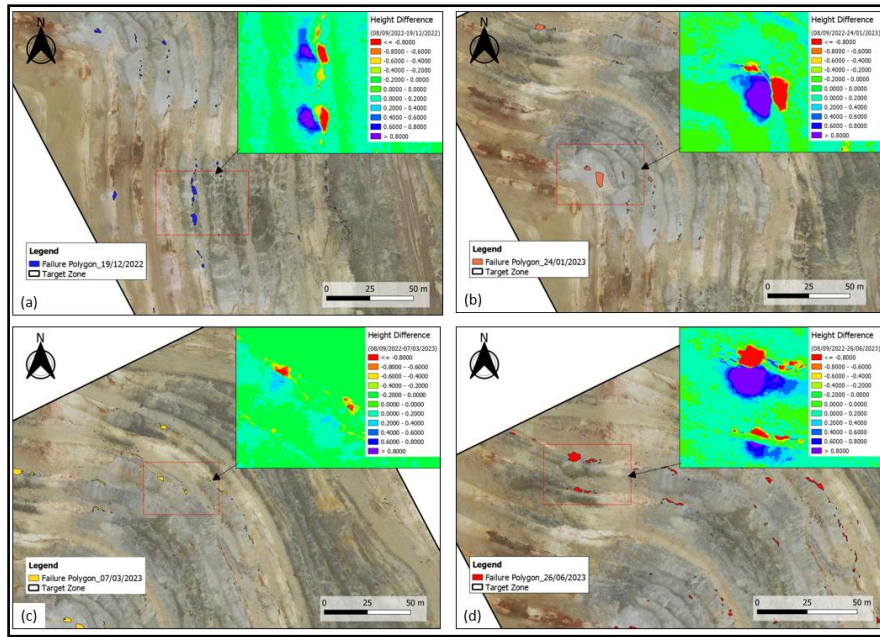


Figure 3.19. Failure polygons acquired from height differences using DEM data between a) 08/09/2022-19/12/2022, b) 08/09/2022-24/01/2023, c) 08/09/2022-07/03/2023, d) 08/09/2022-26/06/2023.

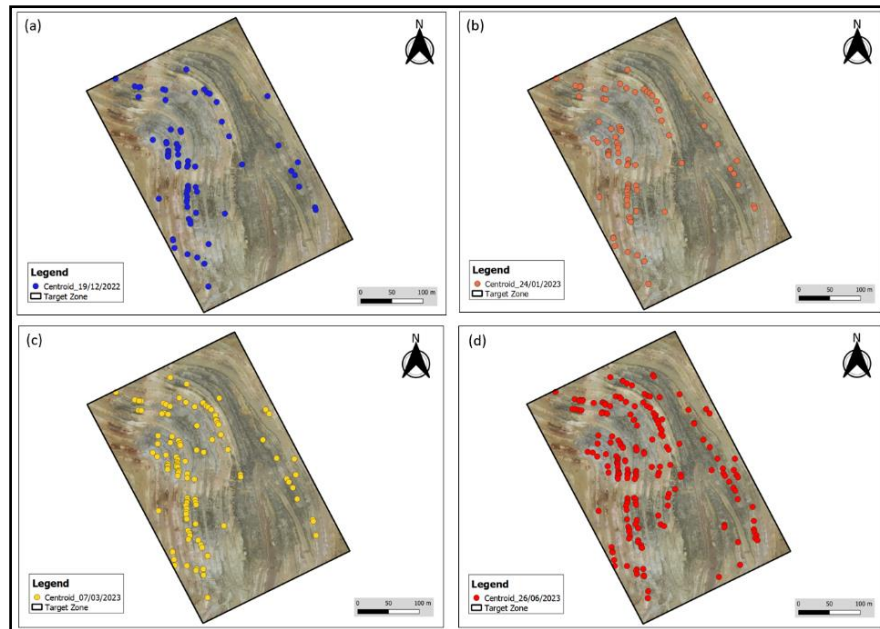


Figure 3.20. Centroid points of failure polygons in the time interval between a) 08/09/2022 – 19/12/2022, b) 08/09/2022 – 24/01/2023, c) 08/09/2022 – 07/03/2023, d) 08/09/2022 – 26/06/2023

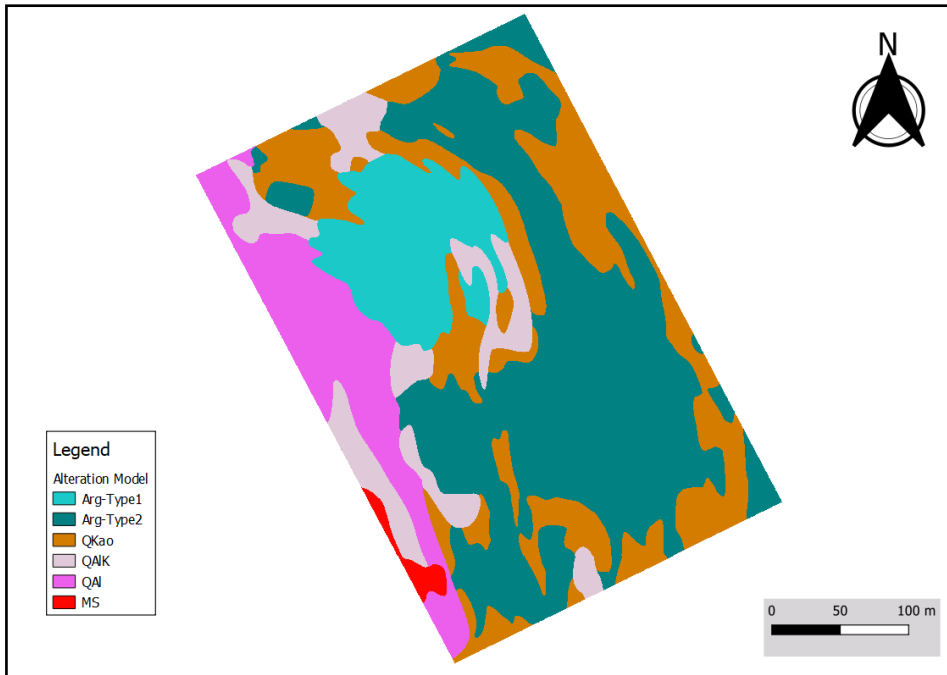


Figure 3.21. Alteration map of the study area

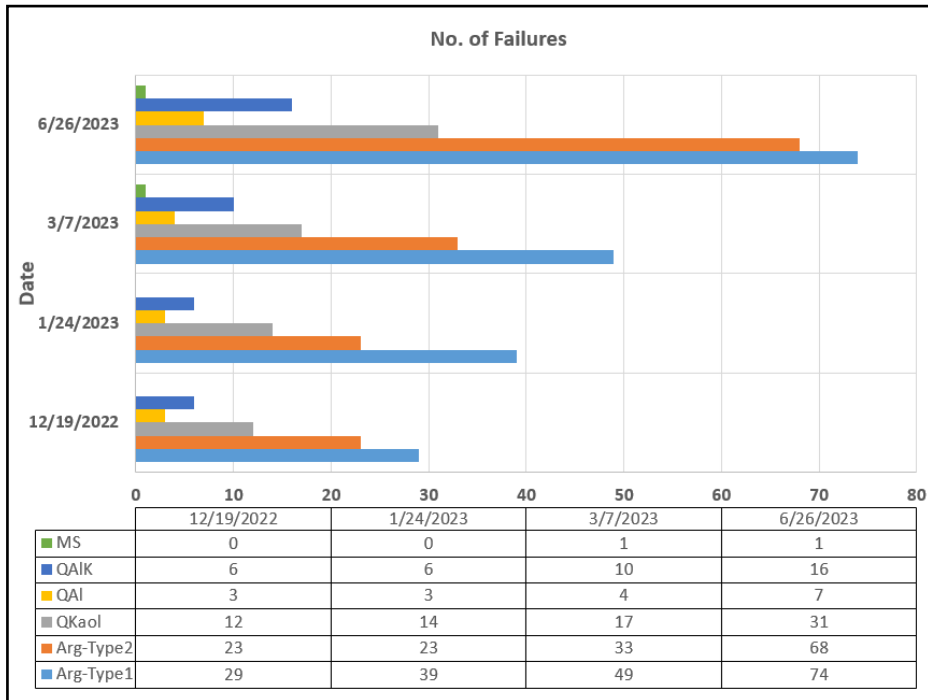


Figure 3.22. Number of centroid points of each failure polygons in each time interval.

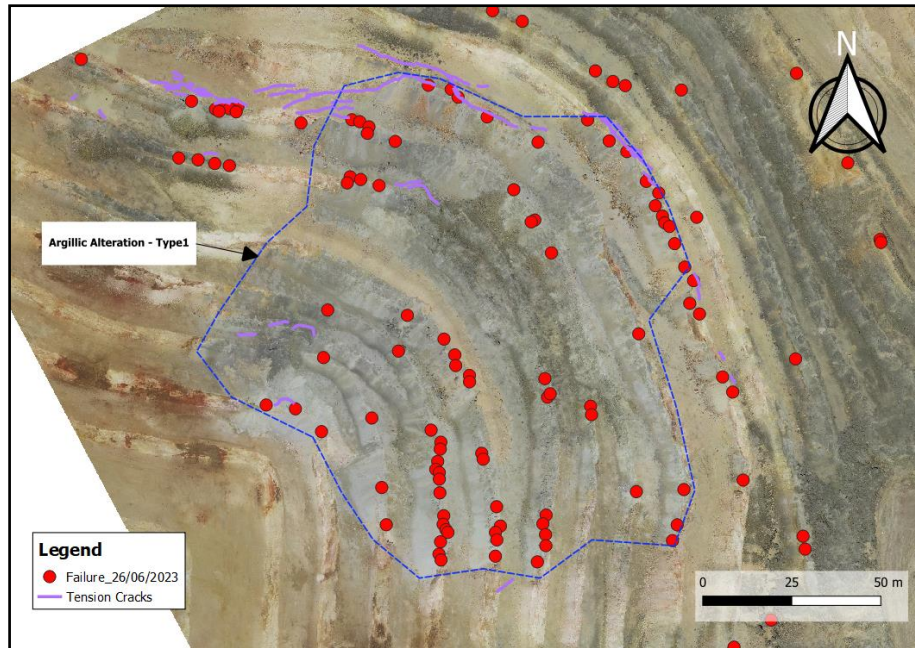


Figure 3.23. The centroid points of failure polygons which belong to last epoch in argillic alteration - type 1 with tension cracks.

3.4.4 Volume Calculation for Deposited Material on the Benches

The materials continuously accumulate on the certain benches in some part of the pit due to the small-scale slope movements. That is why this situation is followed on the orthophotos and elevation differences by using DEM of different epochs. Therefore, six critical areas are detected. Furthermore, the volume calculation is performed by using volume calculation tool plugin in QGIS. Polygon layers and a DEM data of last epoch are used as input layers, and other DEM data is generated using a DTM obtained from survey team in mine site. That DEM data is used as DEM base layer. It is found that the volume values range from 99.8 m³ to 347.7 m³ (Figure 3.24). Especially, the accumulated material covered the benches totally in the areas of A1 and A2 (Figure 3.24), which are in alteration type Arg-Type2 and QAIK.

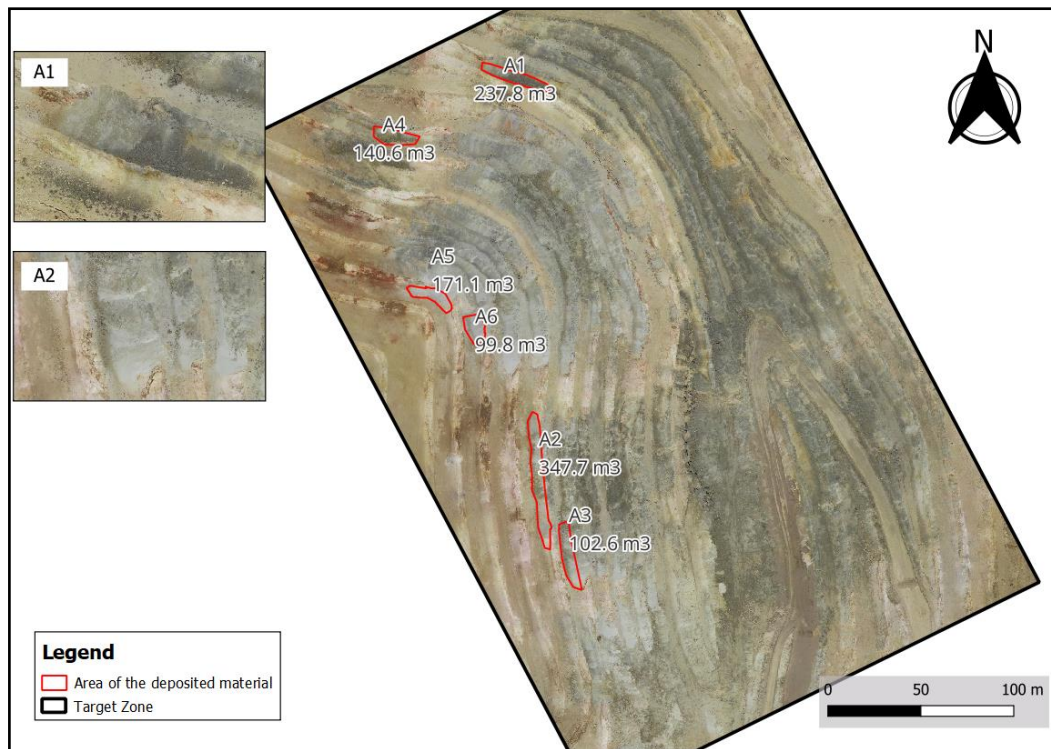


Figure 3.24. Volume calculation of deposited material on the benches.

3.4.5 Tension Crack Mapping

The tension cracks control the slope stability in the pit. Small failures can occur depending on the frequency and the length of tension cracks. Therefore, the tension crack mapping is very important for the evaluation of stability. They are drawn by polyline on the orthophoto of last epoch in QGIS. As shown in figure 3.25, a small failure developed in the dates between 07/03/2023 and 26/06/2023 because of the small tension cracks on the bench at the elevation of 1790 m (Figure 3.25-b). In region 2, the length of the tension cracks is higher than the ones in region 1, and major failures may develop in this zone at the elevation of 1800 m. (Figure 3.25-c). The regions where the tension cracks are concentrated must be monitored carefully to make an estimation of the possible failures that may occur in future.

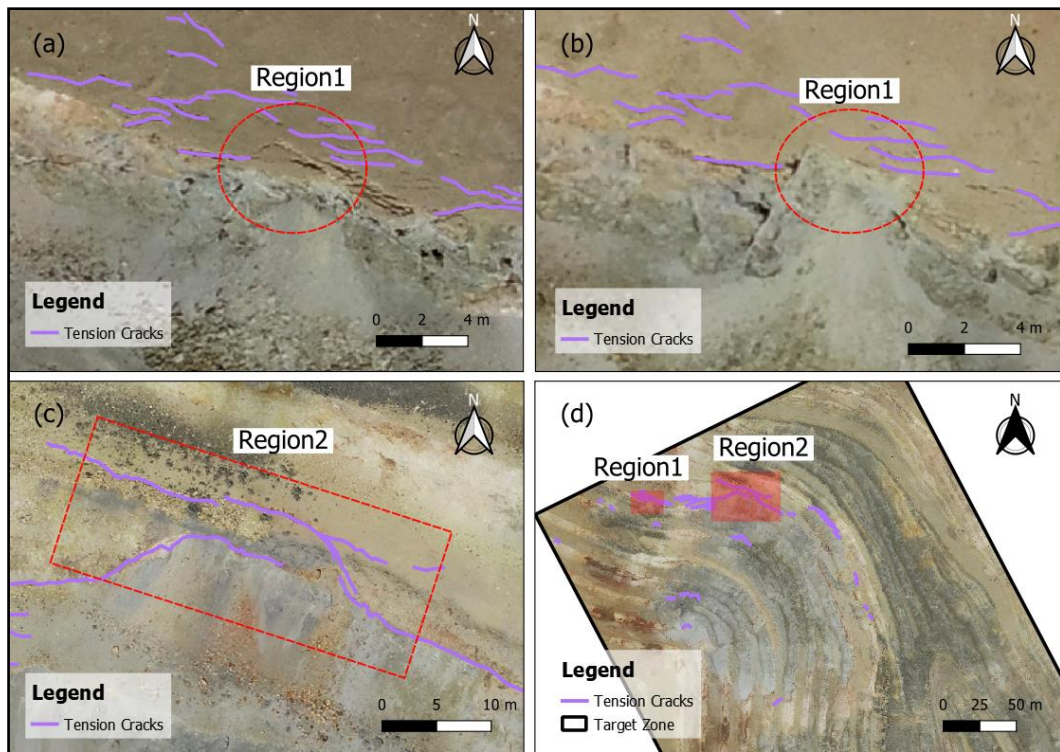


Figure 3.25. a) The distribution of tension cracks around region 1. b) Bench-scale failure caused by the tension crack in region 1. c) The distribution of tension cracks in region 2. d) The overall view of region 1 and region 2.

3.4.6 Creation of Slope Map

Changes in slopes of the pit is very significant to assess the stability as the slopes in this pit are engineered slopes. Firstly, a slope map is generated by using DEM data of last epoch in QGIS software (Figure 3.26-a). The slope map is revised again and bench surfaces are extracted from the existing slope map to remove the accumulated material on the benches and noncritical slopes (Figure 3.26-b). The bench face angles mostly range from min 50 degree to max 65 degree in the pit but the effects of weathering degree or operational mistakes cause the disruption of designed slope angles. When the slope angles are observed in detailed, the regions in which the angle value above 65 degrees are mostly around the contact zones because the

material fails slowly from the upper parts of these regions and designed slopes have been changing in time. That is why the maximum value of 65 degrees is chosen as a limit in the slope map to monitor the status of the slopes.

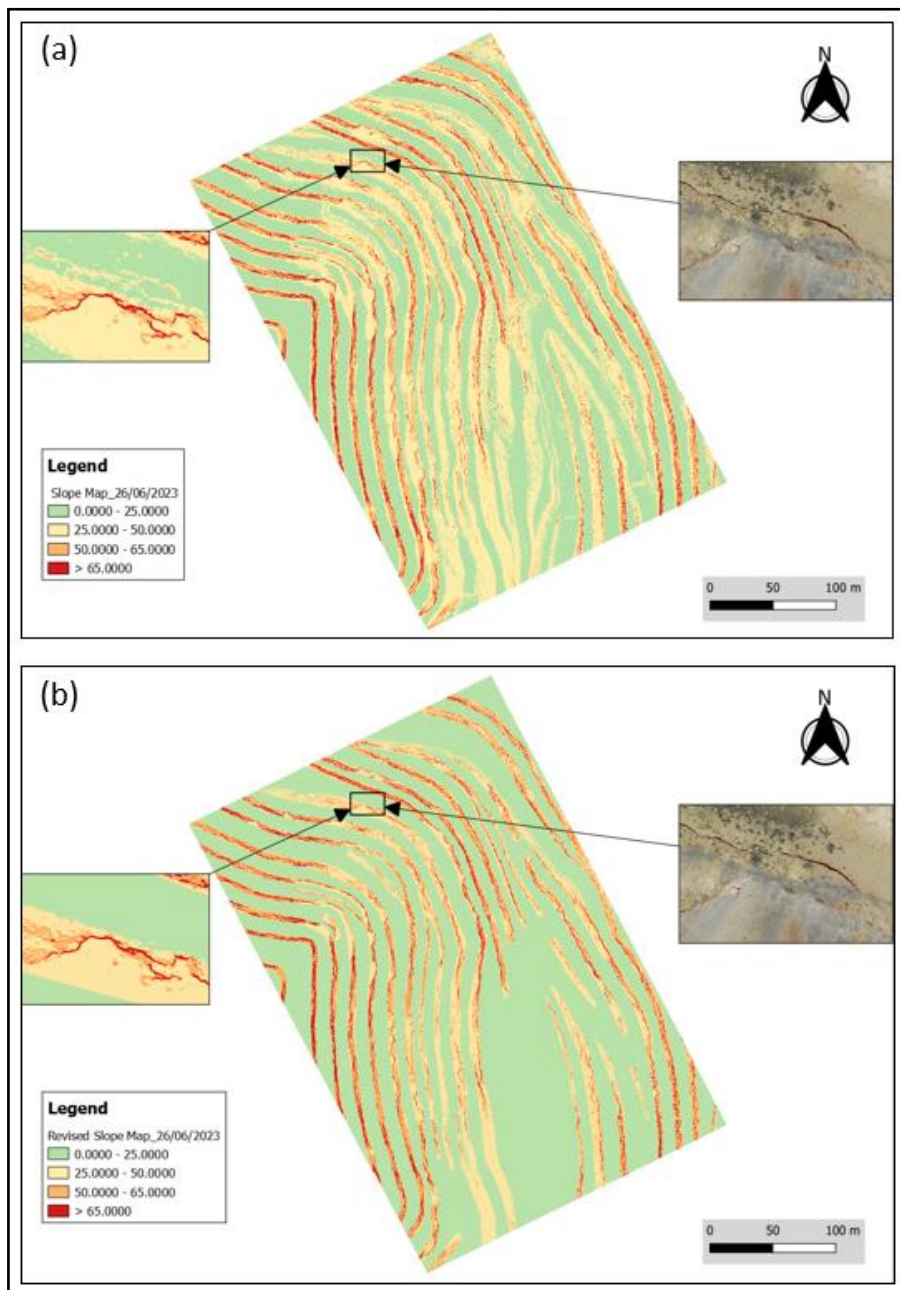


Figure 3.26. a) Slope map generated from DEM of last epoch. b) Revised slope map

CHAPTER 4

INSTABILITY ASSESSMENT MAPPING

After assessment of stability with change detection analysis, a comprehensive map is necessary to see the overall situation of the stability in the study area. Therefore, an instability assessment map is created to specify the susceptible zones by using some significant criteria that may affect the stability in the pit.

The analytical hierarchy process method is applied to create an instability assessment map in QGIS v3.28.8 (*QGIS Desktop 3.28 User Guide QGIS Project, 2023*) which shows the regions prone to next failures based on five criteria such as tension crack, alteration type, slope, volume of the accumulated material, failure concentrations. All these criteria are effective factors which cause instability problems in the pit. The instability assessment map is categorized into five classes like very high, high, medium, low and very low.

4.1 Criteria

a- Alteration Type

The alteration types are categorized into six classes which are argillic, quartz alunite, quartz kaolinite, alunite-kaolinite and massive silica. Argillic alterations are also divided into two classes as argillic type-1 and argillic type-2 because of the differences of weathering degree between two types. The failures are mostly concentrated in the argillic alteration-type1, argillic alteration-type2 and quartz kaolinite respectively whereas the regions of massive silica, quartz alunite and alunite-kaolinite are the more stable classes (Figure 4.1).

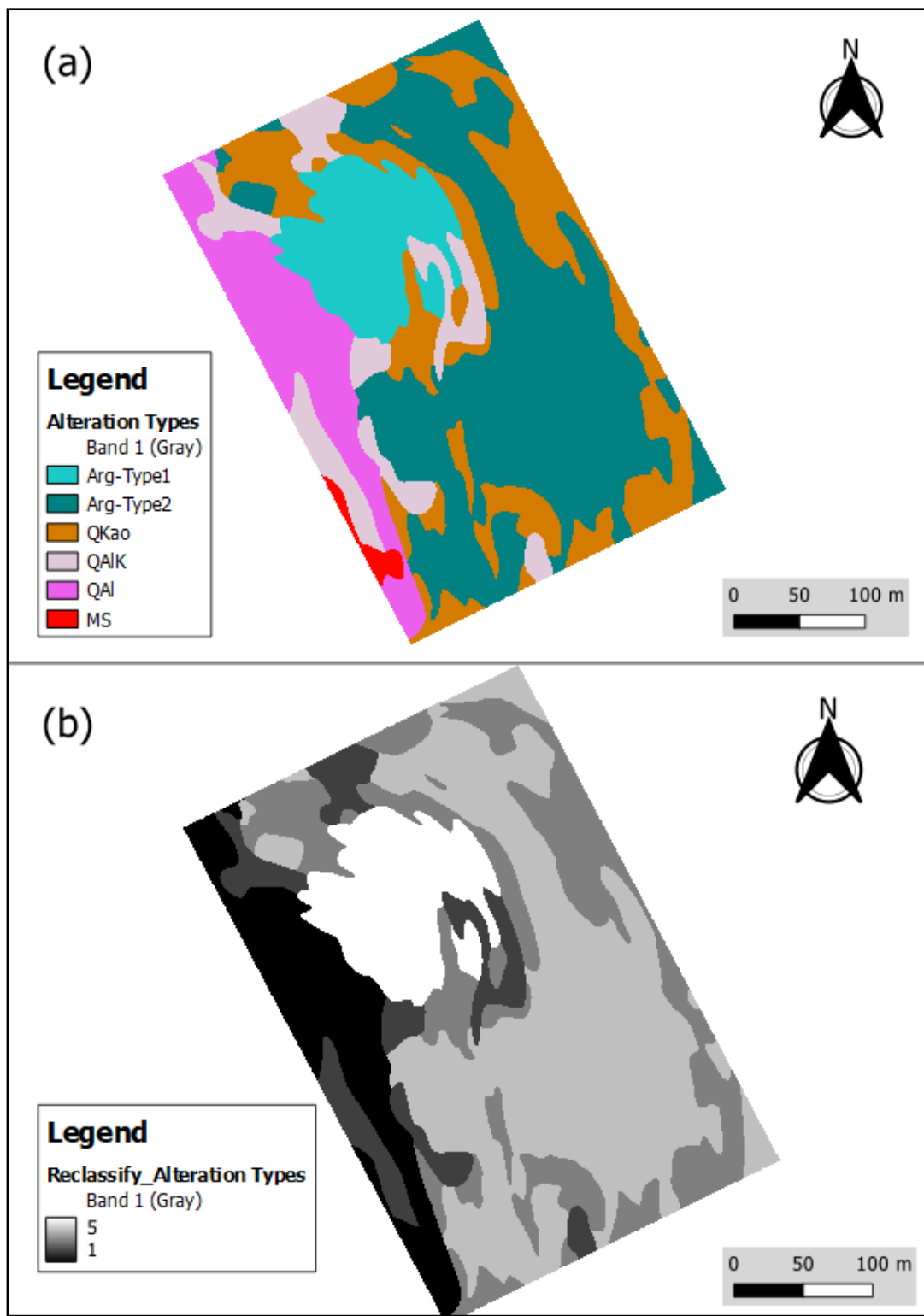


Figure 4.1. a) Alteration type of the study area. b) Reclassified map of Alteration Type.

b- Slope

The slope map is generated by using a digital elevation model which belongs to the latest survey. The slope degrees are categorized into two main groups as “0-65°”, “65°-90°”. The higher score represents the higher bench face angle which is playing an important role to trigger slope instability so that reclassification is performed for assigning the values from 1 to 5 which represents smaller and greater than 65 degree of slope angle respectively (Figure 4.2). The designed slope angles range mostly 50 and 65 degrees, considering different parts and conditions of the pit, 65 degrees are chosen as a limit.

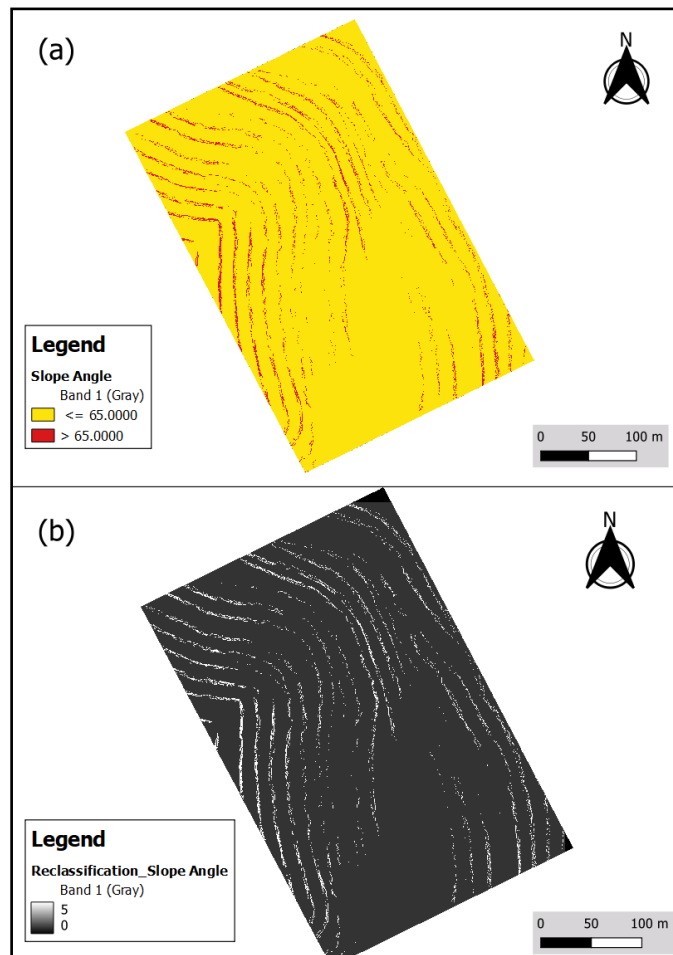


Figure 4.2. a) Raster data of the slope angle. b) Reclassified map of Slope Angle.

c- Tension Crack

The tension cracks concentrated mostly around the argillic alteration-type1. The length of the cracks ranges from 0.74 m to 37.27m, and it is an important factor for the size of the failure that may occur. Therefore, the length is taken as a parameter in *weight field* and search radius is taken as 10 m for the creation of *line density* because the distance of cracks varied between 0.3 - 8 m. Afterwards, the values are classified into five intervals from 1 to 5 by using *Reclassify by Table* plugin (Figure 4.3). In this way, the highest score represents the regions in which the longer and concentrated cracks are present.

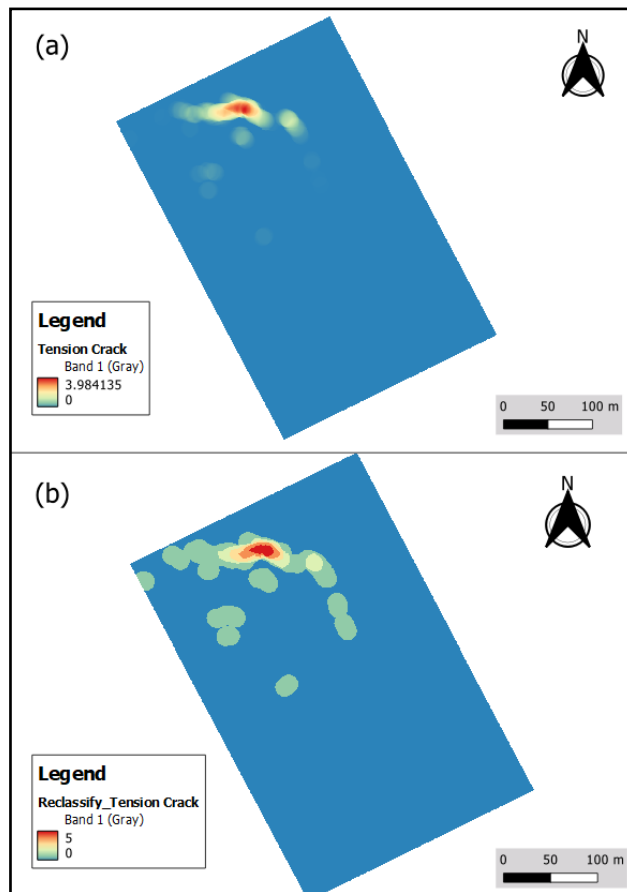


Figure 4.3. a) Kernel density estimation of tension crack. b) Reclassified map of tension crack.

d- Volume of Accumulated Material

Some failures repeatedly occur in the same previous failure locations which cause the accumulation of material on the bench just below in time. The accumulated materials may result in new failures in future depending on the volume of deposition. Thus, the volume calculation is taken into consideration as a factor that may affect stabilization. *Volume Calculation Tool* is used for the volume calculation of each material in determined areas. Six regions of some accumulated materials are drawn manually by polygon first (Figure 3.23). Then, DEM layer of last survey is selected in *DEM Height Layer*, and an existing raster data derived from DTM is chosen in *DEM Base Layer* (Figure 4.4).

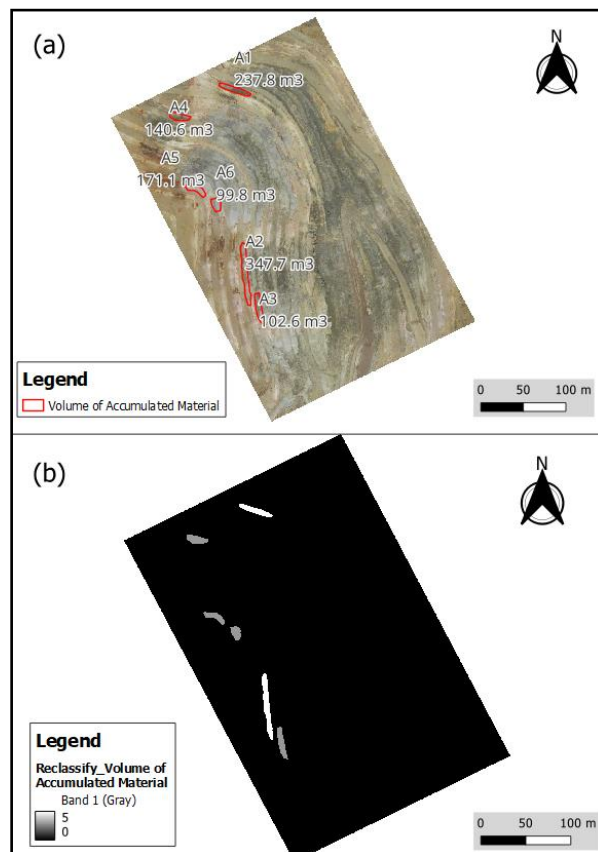


Figure 4.4. a) Vector data of the volume of accumulated material. b) Reclassified map of the volume of accumulated material.

e- Failure Concentration

The failure locations derived from last DEM data are firstly vectorized as polygons and each failure polygon's failure area information is recorded in the attribute table. Second step is to form centroid points of these polygons to use those point data in heatmap. Finally, the vectorized centroid data is taken as the input layer, the radius as selected 50 meters because the diameter of change rates varied between 18-40 m and a radius of 50 m was chosen to generalize the representation of the distance between these deformations, and the *area* field is selected for *weight from field option* as advanced parameters in the *Heatmap* plugin. As a result, a density raster is acquired to represent the regions weighted with the magnitude of the failure areas (Figure 4.5).

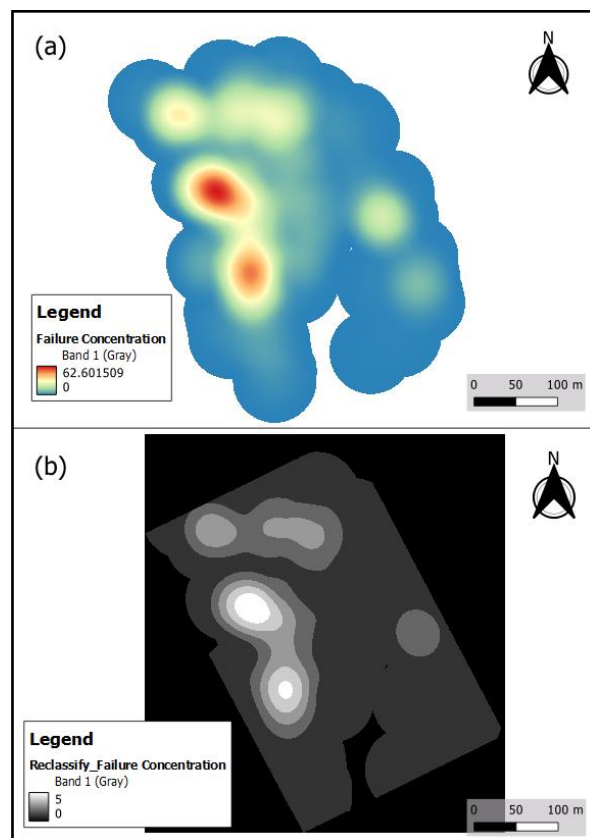


Figure 4.5. a) Raster data of failure concentration. b) Reclassified map of failure concentration.

All criteria classification and reclassification values are summarized in table 4.1. The higher reclassification values define negative effects and risky situations on the stability.

Table 4.1 Summary of the classification and reclassification details of the criteria

Criteria	Classification	Reclassification Value
Volume of Accumulated Material	0 - 200	3
	200 - 400	5
Alteration Type	Arg-Type1	5
	Arg-Type2	4
	QKao	3
	QAiK	2
	QAi	1
	MS	1
Slope	0 - 65	1
	65 - 90	5
Tension Crack	0 – 0.8	1
	0.8 – 1.4	2
	1.4 – 2.2	3
	2.2 – 3.0	4
	3.0 – 3.98	5
Failure Concentration	0 - 12.6	1
	12.6 - 25.2	2
	25.2 - 38.6	3
	38.6 - 50.2	4
	50.2 – 62.60	5

4.2 Creation of Instability Assessment Map in QGIS

As a result, five criteria are taken into consideration to perform the analytical hierarchy process method. The weighted values of the criteria are assigned 0.466 for alteration type, 0.316 for tension crack, 0.116 for failure concentration, 0.064 for

volume of accumulated material, 0.038 for slope as a result of pairwise comparison matrix (Table 4.2). The instability assessment map is created through raster calculator in QGIS (Figure 4.6). The map is divided into five classes based on equal interval to define class interval. The summary information about the data with descriptions for the instability assessment map is shown in table 4.3.

Table 4.2 Pairwise Comparison Matrix for the datasets and criteria weight results

Factors	<i>(1)</i>	<i>(2)</i>	<i>(3)</i>	<i>(4)</i>	<i>(5)</i>	Criteria Weight	Criteria Weight %
(1) Alteration Type	1	2	3	3	4	0.383	38.3
(2) Tension Crack	1/2	1	3	3	3	0.275	27.5
(3) Failure Concentration	1/3	1/3	1	3	2	0.160	16.0
(4) Slope	1/3	1/3	1/3	1	2	0.105	10.5
(5) Volume of Deposited Material	1/4	1/3	1/2	1/2	1	0.076	7.6
Total						1	100
Consistency ratio:	0.057						

Table 4.3 Descriptions and their class intervals for Instability Assessment Map

Description	Class Value
Very Low	< = 1.25
Low	1.25 – 2.01
Medium	2.01 – 2.77
High	2.77 – 3.53
Very High	= > 3.53

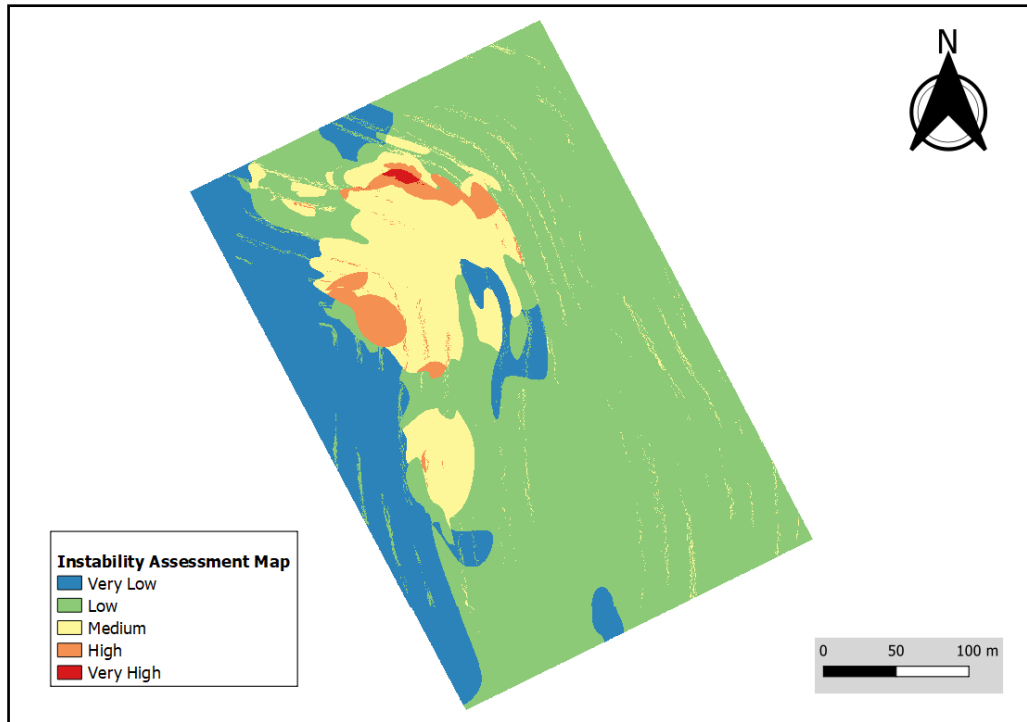


Figure 4.6. Instability Assessment Map.

4.3 Accuracy Assessment of Instability Assessment Map

The instability assessment map, which could be considered as a special type of a susceptibility map for engineered mining slopes, is assessed with the failure polygons of last epoch. The classes of instability assessment map are transferred to attribute tables of each failure polygon as new attributes and then for each instability assessment map class the areal densities of failure polygons are calculated by using both the areas of failure polygons and areas of respective instability assessment map class. Figure 4.7 present that the density of failures which are used as ground truth or accuracy assessment set, is exponentially increasing through high and very high classes, which indicate that the MCDA constructed for instability assessment map is relatively accurate.

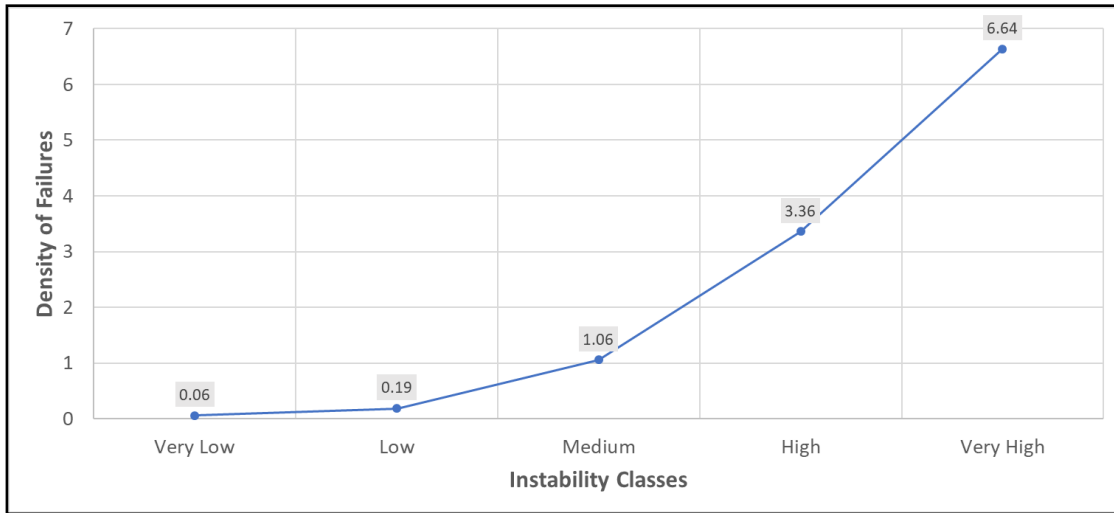


Figure 4.7. Accuracy Assessment of Instability Assessment Map.

CHAPTER 5

RESULTS AND DISCUSSION

5.1 Change Detection Analyses

Change detection analyses are performed by using five point cloud sets to see the stability problems in the pit. As a result of these analyses, it is clearly seen that the instability issues are in the bench-scale within 291 days. The maximum displacement is -2.41 m while the average displacement is -0.03 m with respect to the last comparison (Figure 3.10).

5.2 The Volume Calculation for Accumulated Material

The volume accumulation is taken into consideration in this study to use it as a criterion for the creation of instability assessment mapping. The volume values range from 99.8 m³ to 347.7 m³ in six significant areas which are previously determined in data analyses section (Figure 3.24). Especially, the accumulated materials cover the benches completely in the area of A1 and A2, and exceed the border of the benches and fell down on one more bench below.

5.3 Types of Alteration

The alteration types in the pit play an important role in the stability. According to the location of failures in all surveys, it can be clearly seen that argillic material (AR) is the alteration type in the failures that mostly occur while Massive Silica (MS) and Quartz-Alunite (QAl) are the higher stable alterations (Figure 3.22).

5.4 Performance of Low-Cost UAV to monitor Mining Sites

In the absence of the expensive monitoring tools like SSR or in the situations of a breakdown in the devices, low-cost UAV systems can play an important role in monitoring mining sites. As mentioned in section 3.4, it is clearly seen that the drone used on the site enables an opportunity to make deformation analysis. In addition, the advantages of drone surveying are detection of the possible failures with the frequency status and magnitudes values, possible tension cracks that may develop on the benches, observing movements in different types of lithology or alterations, following the effects of bench face angles for stability assessment in the desired time interval. Besides the deformation analysis, Drone surveying can allow the engineers to create a comprehensive map based on the principles of multicriteria decision making, and it is very useful to evaluate overall stability and all risky situations by using various datasets derived from UAV in a single map.

The weather conditions can affect the drone surveying in a specific time interval. For instance, the unsuitable weather conditions like snowy, rainy, or windy may limit the use of low-cost UAV systems but they are very powerful tools to provide qualified information or data to evaluate the stability of the mining sites in proper weather and climate conditions.

There are some disadvantages of low-cost drone monitoring like long time for obtaining the data from field and processing them in the office. Therefore, the side and forward overlap ratios are chosen 60% to complete field works with a single battery in 26 minutes. In addition to that, the value ratios enable smaller number of photos to speed up the photogrammetry process for office works in this study. The ratio value of 60% is good enough to provide overlap properly, and it shortens duration of the field and office works efficiently. In any case, the low-cost drone monitoring takes some time compared to the expensive monitoring tools like SSR which receives instant data for 24 hours.

5.5 Stability Status on Different Types of Alteration

When observing the orthomosaics in detail, it is easily noticed that weathering degree is quite effective in stability issues in Arg-Type1 whereas discontinuity sets play an important role in creation of bench-scale failures in Arg-Type2. Especially flow layers in Arg-Type2 are dipping through west direction, which pose a risk for stability on steep slopes in bad weather conditions. The frequency of failures is higher in Arg-Type1 than the other types, and these failures are in bench-scale at the moment, but this situation may develop into larger deformation within the bounds of this alteration type in later stages.

5.6 Negative Effects of Tension Cracks on Slope Stability

Tension cracks are responsible factor for the instability issues in the pit. Small bench-scale failures occurred on site because of the progressive development of tension cracks as shown in data analyses section. When underlying material (Arg-Type1) decomposes, just above that bench tension cracks develop and pose a risk for slope stability. Therefore, they are used as a causative criterion for the creation of instability assessment map. The longer tension cracks, the higher risk for slope stability, hence the parameter is calculated as length weighted. The regions where tension cracks are concentrated must be monitored carefully to make an estimation of the possible failures that may occur in future by considering the weathering conditions.

5.7 The Volume Accumulation on the Benches

A1 and A2 areas seem to be critical because the deposited material covers benches totally, even exceeding the border of benches and fell down on one more bench below (Figure 3.23). The accumulated materials should be removed regularly to provide the slope stability and to keep the structures as designed.

CHAPTER 6

CONCLUSION

The deformation analyses are performed with point cloud comparisons in the mining site, and it is proven that the small-scale failures are detected easily with low-cost drone technology. This provides a regular monitoring with low-cost UAV effectively in a specific time interval. In addition, the study enables to detect the unstable alteration type that cause the stability issues. Besides this, the tension cracks developed on the site are mapped and their negative effects on the stability are followed efficiently. The volume of the accumulated material on the desired benches is calculated, and it enables the geotechnical engineers to find the locations where cleaning process is necessary. The negative factors alteration type, tension crack, failure concentration, the volume of the accumulated material and slope are used to create an instability assessment map, and it enables to observe the risky parts of the study area with UAV. As conclusion, low-cost UAV technology is one of the powerful tools to monitor a mine site in an efficient and reliable way.

REFERENCES

- Agisoft Metashape User Manual Professional Edition, Version 2.0.* (2023).
- Ahmad Fuad, N., Yusoff, A. R., Ismail, Z., & Majid, Z. (2018). Comparing the performance of point cloud registration methods for landslide monitoring using mobile laser scanning data. *International Archives of the Photogrammetry, Remote Sensing and Spatial Information Sciences - ISPRS Archives*, 42(4/W9), 11–21. <https://doi.org/10.5194/isprs-archives-XLII-4-W9-11-2018>
- Aluç, A., Kuşcu, İ., Peytcheva, I., Cihan, M., & von Quadt, A. (2020). The late Miocene Öksüt high sulfidation epithermal Au-Cu deposit, Central Anatolia, Turkey: Geology, geochronology, and geochemistry. *Ore Geology Reviews*, 126. <https://doi.org/10.1016/j.oregeorev.2020.103795>
- Basharat, M., Shah, H. R., & Hameed, N. (2016). Landslide susceptibility mapping using GIS and weighted overlay method: a case study from NW Himalayas, Pakistan. *Arabian Journal of Geosciences*, 9(4). <https://doi.org/10.1007/s12517-016-2308-y>
- Bhagya, S. B., Sumi, A. S., Balaji, S., Danumah, J. H., Costache, R., Rajaneesh, A., Gokul, A., Chandrasenan, C. P., Quevedo, R. P., Johnny, A., Sajinkumar, K. S., Saha, S., Ajin, R. S., Mammen, P. C., Abdelrahman, K., Fnais, M. S., & Abioui, M. (2023). Landslide Susceptibility Assessment of a Part of the Western Ghats (India) Employing the AHP and F-AHP Models and Comparison with Existing Susceptibility Maps. *Land*, 12(2). <https://doi.org/10.3390/land12020468>
- Cook, K. L. (2017). An evaluation of the effectiveness of low-cost UAVs and structure from motion for geomorphic change detection. *Geomorphology*, 278, 195–208. <https://doi.org/10.1016/j.geomorph.2016.11.009>
- Devara, M., Tiwari, A., & Dwivedi, R. (2021). Landslide susceptibility mapping using MT-InSAR and AHP enabled GIS-based multi-criteria decision analysis. *Geomatics, Natural Hazards and Risk*, 12(1), 675–693. <https://doi.org/10.1080/19475705.2021.1887939>
- El Jazouli, A., Barakat, A., & Khellouk, R. (2019). GIS-multicriteria evaluation using AHP for landslide susceptibility mapping in Oum Er Rbia high basin (Morocco). *Geoenvironmental Disasters*, 6(1). <https://doi.org/10.1186/s40677-019-0119-7>
- Esposito, G., Salvini, R., Matano, F., Sacchi, M., Danzi, M., Somma, R., & Troise, C. (2017). Multitemporal monitoring of a coastal landslide through SfM-derived point cloud comparison. *Photogrammetric Record*, 32(160), 459–479. <https://doi.org/10.1111/phor.12218>
- Feizizadeh, B., & Blaschke, T. (2013). GIS-multicriteria decision analysis for landslide susceptibility mapping: Comparing three methods for the Urmia lake basin, Iran. *Natural Hazards*, 65(3), 2105–2128. <https://doi.org/10.1007/s11069-012-0463-3>

- Hajduk, S. (2022). Multi-Criteria Analysis in the Decision-Making Approach for the Linear Ordering of Urban Transport Based on TOPSIS Technique. *Energies*, 15(1). <https://doi.org/10.3390/en15010274>
- Hayakawa, Y. S., & Obanawa, H. (2020). Volumetric change detection in bedrock coastal cliffs using terrestrial laser scanning and uas-based SFM. *Sensors (Switzerland)*, 20(12), 1–16. <https://doi.org/10.3390/s20123403>
- Kyriou, A., Nikolakopoulos, K. G., & Koukouvelas, I. K. (2022). Timely and Low-Cost Remote Sensing Practices for the Assessment of Landslide Activity in the Service of Hazard Management. *Remote Sensing*, 14(19). <https://doi.org/10.3390/rs14194745>
- Lague, D., Brodu, N., & Leroux, J. (2013). Accurate 3D comparison of complex topography with terrestrial laser scanner: Application to the Rangitikei canyon (N-Z). *ISPRS Journal of Photogrammetry and Remote Sensing*, 82, 10–26. <https://doi.org/10.1016/j.isprsjprs.2013.04.009>
- Malczewski, J. (1999) GIS and Multicriteria Decision Analysis. John Wiley and Sons, Inc., New York.
- Malczewski, J. (2000). On the use of weighted linear combination method in GIS: Common and best practice approaches. *Transactions in GIS*, 4(1), 5–22. <https://doi.org/10.1111/1467-9671.00035>
- Osasan, K. S., & Afeni, T. B. (2010). REVIEW OF SURFACE MINE SLOPE MONITORING TECHNIQUES. In *Journal of Mining Science* (Vol. 46, Issue 2).
- Paradella, W. R., Ferretti, A., Mura, J. C., Colombo, D., Gama, F. F., Tamburini, A., Santos, A. R., Novali, F., Galo, M., Camargo, P. O., Silva, A. Q., Silva, G. G., Silva, A., & Gomes, L. L. (2015). Mapping surface deformation in open pit iron mines of Carajás Province (Amazon Region) using an integrated SAR analysis. *Engineering Geology*, 193, 61–78. <https://doi.org/10.1016/j.enggeo.2015.04.015>
- QGIS Desktop 3.28 User Guide QGIS Project.* (2023).
- Ren, H., Zhao, Y., Xiao, W., & Hu, Z. (2019). A review of UAV monitoring in mining areas: current status and future perspectives. In *International Journal of Coal Science and Technology* (Vol. 6, Issue 3, pp. 320–333). Springer International Publishing. <https://doi.org/10.1007/s40789-019-00264-5>
- Saaty, R. W. (1987). *THE ANALYTIC HIERARCHY PROCESS-WHAT IT IS AND HOW IT IS USED* (Vol. 9, Issue 5).
- Singh, A. (1989) Review Article Digital Change Detection Techniques Using Remotely-Sensed Data. *International journal of remote sensing*, 10, 989-1003. <https://doi.org/10.1080/01431168908903939>
- Taherdoost, H., & Madanchian, M. (2023). Multi-Criteria Decision Making (MCDM) Methods and Concepts. *Encyclopedia*, 3(1), 77–87. <https://doi.org/10.3390/encyclopedia3010006>
- Teo, T. A., Fu, Y. J., Li, K. W., Weng, M. C., & Yang, C. M. (2023). Comparison between image- and surface-derived displacement fields for landslide monitoring using an

- unmanned aerial vehicle. In *International Journal of Applied Earth Observation and Geoinformation* (Vol. 116). Elsevier B.V. <https://doi.org/10.1016/j.jag.2022.103164>
- Vaziri, A., Moore, L., & Ali, H. (2010). Monitoring systems for warning impending failures in slopes and open pit mines. *Natural Hazards*, 55, 501–512. <https://doi.org/10.1007/s11069-010-9542-5>
- Yager, R. R. (1988). On ordered weighted averaging aggregation operators in multicriteria decisionmaking. *IEEE Transactions on Systems, Man, and Cybernetics*, 18(1), 183–190. <https://doi.org/10.1109/21.87068>
- Yeon, Y. K., Han, J. G., & Ryu, K. H. (2010). Landslide susceptibility mapping in Injae, Korea, using a decision tree. *Engineering Geology*, 116(3–4), 274–283. <https://doi.org/10.1016/j.enggeo.2010.09.009>
- Younger, P. (2007). Mining and its impact on the environment, by F.G. Bell and L.J. Donnelly. Taylor & Francis, London. 547pp. 2006. Hardback 80. *Quarterly Journal of Engineering Geology and Hydrogeology - Q J ENG GEOL HYDROGEOL*, 40, 310–311. <https://doi.org/10.1144/1470-9236/07-109>